MB

Institute of Neurology
(Queen Square)
University College London

Probabilistic tractography of the whole telencephalic corticospinal tract as a predictive marker of motor recovery in chronic stroke patients

Giovanni Antonio Cocco, MD

Supervision of

Dr Nick Ward (Department of Brain Repair and Rehabilitation, ION)

Dr Chris Clark (Institute of Child Health)

Submitted as partial fulfilment of the requirements for the MSc in Clinical Neurology, University of London

Year of Submission: 2008

Word Count: 10076

MSc Clinical Neurology
2007/08

ProQuest LLC
789 East Eisenhower Parkway
P.O. Box 1346
Ann Arbor, MI 48106-1346

Contents

To my family

Acknowledgments

My warmest thanks to my supervisors, Dr Nick Ward and Dr Chris Clark, who offered me to take part in this study, allowing me to move my first steps in research through tractography. I am grateful to them for being tireless in answering my questions and for being patient when dealing with my ignorance. Working with them is a privilege and a pleasure.

I am indebted with Dr Jon Clayden and Dr Bogdan Draganski. I had to disturb Jon several times per day whenever I was not able to manage by myself all the problems and difficulties I met while learning the software needed to process diffusion images; unfortunately for him, it happened quite often, and he never denied his help.
Regarding Bogdan, he has always found the time to assist and helping me in several steps of this project. I am so sorry he probably will not go on working in the Institute of Neurology in the next months; it will be difficult to find another colleague so brilliant in explaining the most difficult concepts of diffusion images. I wish him all the best for his career.
An important support was given also by the CAMINO group, especially by Dr Philip Cook: I never saw him, but his help through his emails has been crucial.

I am thankful to Dr Alex Leff for his advice throughout this year and to Prof. Simon Shorvon and Dr Caroline Selai, for organizing this great course.
Thanks to all the colleagues of the course, who rendered pleasant all the hours spent in the Institute, and most of those spent outside. I learned enormously from them, not only from their knowledge of neurology, but from their different cultures and background as well.

I would like say thanks not only to Dr Caroline Selai again, but to Dr Daniela Warr and Dr Barbara Harder as well, who gave me a great assistance in having the possibility to attend the Master in Advanced Neuroimaging next year. I am confident it will be another wonderful course.

Finally, many thanks to my family for their unconditional love and support, and to the friends and colleagues of the Neurological Clinic of Sassari, in particular Prof. GianPietro Sechi, from whom I started to learn neurology.

List of abbreviations

- 9HPT: 9-Hole Peg Test
- ADC: Apparent Diffusion Coefficient
- AMT: Active motor thresholds
- ARAT: Action Research Arm Test
- Aslope: Slope of recruitment curve during background contraction
- CST: Corticospinal tract
- DTI: Diffusion tensor imaging
- DWMRI: Diffusion-weighted magnetic resonance imaging
- EMG: Electromyography
- FA: Fractional anisotropy
- FAratio: FA value resulting from the ratio of (unaffected CST - affected CST) / (unaffected CST + affected CST)
- FDI: First dorsal interossei
- fMRI: Functional MRI
- GRIP: Maximum grip strength test
- JTT: Jebsen-Taylor Hand Function Test
- MAX: Maximal MEP amplitude recorded during the acquisition of the RC
- MaxC: Unthresholded maximum connectivity map
- MeanC: Unthresholded mean connectivity map
- MEG: Magnetoencephalography
- MEP: Motor evoked potentials
- MER: Motor evoked response
- MNI: Montreal neurological institute
- MRI: Magnetic resonance imaging
- MVC: Maximum voluntary contraction
- PDF: Probability density functions
- PICo: Probabilistic Index of Connectivity
- RC: Recruitment curve during background contraction
- rMT: Resting motor threshold
- ROI: Region of interest
- rpFA: Affected CST FA value/unaffected CST FA value in patients
- TMaxC: Thresholded maximum connectivity maps
- TMeanC: Thresholded mean connectivity map
- TMS: Transcranial magnetic stimulation

Abstract

Background: Probabilistic tractography provides a voxel-based connectivity index that reflects fibre organisation and integrity. We aim to quantify the integrity of the whole telencephalic portion of the corticospinal bundle as assessed by probabilistic tractography in patients who suffered from stroke; and to investigate whether the integrity of the corticospinal bundle, as assessed by probabilistic tractography, correlates with: (i) the cortical-spinal system integrity as assessed by TMS, (ii) the degree of motor impairment and/or (iii) the degree of functional improvement achieved by the patients during a two week period of intensive upper limb training.

Methods: Ten patients chronic stroke patients, in whom weakness of at least wrist and finger extensors and hand interossei was present for at least 48 hours after the onset of the symptomatology of their first-ever stroke, were assessed at least one year later through traditional MRI and diffusion tensor imaging. 9 age-matched controls were also scanned. Patients underwent a two weeks intensive physiotherapy treatment of the upper limb as part of a separate clinical trial. Imaging data were acquired prior to the treatment period. Neurophysiological data and motor impairment scores were also acquired immediately before and after the treatment period.

Results: Fractional anisotropy values of the whole telencephalic portion of the corticospinal bundle were able to distinguish between affected and not affected tracts. Moreover, in spite of the small number of patients investigated till now, FA values calculated on the whole telencephalic corticospinal tract seems able to predict the recovery after the rehabilitation treatment.

Conclusions: Probabilistic tractography is a useful measure for detecting differences in the affected and unaffected corticospinal bundle, reflecting the fibres disruption consequent to a stroke lesion.
A largely automated protocol for the tracking of corticospinal bundle is presented, with the aim to reduce the bias dependent from the manual drawing of the region of interest. Preliminary observations and considerations about the reliability of the various values of fractional anisotropy (calculated through probabilistic tractography in the whole telencephalic corticospinal tract) in predicting the degree of motor impairment and post rehabilitation recovery are discussed.

Introduction

Stroke, or brain attack, occurs when a region of the brain does not receive a sufficient blood flow, resulting in death of cerebral tissue. It is the third most common cause of death and the first cause of long-term adult disability (1).

Stroke risk factors are distinguished in modifiable or not-modifiable ones. Among the modifiable ones, hypertension, hyperlipidemia, diabetes, atrial fibrillation and cigarette smoking are the most frequent (2), whilst age, gender, ethnicity, and heredity are the most important not-modifiable risk factors (3).

Stroke can be divided into two main categories, according to the underlying pathophysiology: ischemic stroke and haemorrhagic stroke. A more severe neurological impairment during the acute phase and a higher mortality rate is observed in patients affected by a haemorrhagic stroke compared to those who had an ischemic stroke (4).

The social burden of stroke is related to its consequent disability as well: it was calculated stroke –related disability is the sixth most common cause of reduced autonomy in the population (5) but, since mean age and life expectancy is predicted to rise in western countries, stroke will rank to the fourth cause of disability (6).

It can be certainly stated that, from the 130,000 stroke cases which happen every year in United Kingdom, a large rate of survivors will be left with some degree of disability (7).

It is common as well to observe a partial or, less frequently, a complete recovery after the acute phase, over the following months; since it cannot be reasonably related only to the resolution of acute changes related to the insult

(e.g. surrounding lesion oedema, acute cerebral choc etc.), a subsequent posttraumatic "reorganization" of cerebral architecture is supposed to play a relevant role. The brain ability of changing its structure and function in order to challenge new experiences, carry on new tasks or go on performing old ones remedying to a recent insult is usually termed "brain plasticity" (8).

It is worth noting that motor control has a bihemispheric localization during childhood, whereas it becomes mainly controlateral (at least in the case of primary motor cortex) to movement during adulthood. Transcranial magnetic stimulation (TMS) studies demonstrated the elicitation of ipsilateral motor evoked potentials (MEPs) in two-thirds of a children group younger than 10 years-old, more often in proximal than in distal muscles. MEPs could not be detected anymore after the age of 10 and in adults (9).

However, even if homolateral motor control probably is not that paramount in physiological conditions during the adulthood, some evidence suggests that its integrity is pivotal in determining a degree of recovery after subcortical stroke (10).

A post-stroke reorganisation of the ipsi- and controlesional cerebral cortex, in particular of the motor areas, has been identified by different authors with different techniques like functional MRI (fMRI), TMS and magnetoencephalography (MEG) (11-13) but its kind of pattern able to predict or, at least, to describe the degree of recovery in a motor-impaired patients who suffered from stroke is at least controversial: it is commonly accepted that the activation areas of the brain are wider (in ipsi- and controlesional hemispheres) during movement, but if it reflects the attempt or rather the failure of the

damaged brain in reorganizing an effective cerebral motor pathway is unclear (13) .

The integrity of the corticospinal tract (CST) as a predictive measure of the potential recovery after a stroke appears to be less controversial.

In 2006 Ward described the fMRI, TMS and behavioural motor findings in 8 patients who suffered from their first-ever stroke resulting acutely in weakness of at least wrist and fingers extensors and hand interossei.

A negative correlation between the gradient of stimulus/response curve and the activation of several motor-related areas was observed. This finding could be interpreted as an attempt of the damaged brain to find another pathway to send the motor output to the periphery bypassing the disrupted CST (14).

Regarding this point, an interesting paper from Stinear was published in 2007: the CST functional integrity was assessed through TMS, fMRI and internal capsule fractional anisotropy (FA) in 21 chronic stroke patients (at least 6 months after the event): patients without a motor evoked response (MER) at the TMS and with a FA asymmetry between the affected and the unaffected CST (a measure which reflects the disruption of the corticospinal system) superior to 0.25 did not show any meaningful motor gains in the following months (15).

It can be stated that, whatever effective the cerebral cortex reorganization following a stroke can be, the clinical motor recovery in the following months requires first of all the integrity of the corticospinal system. In other words, even if other areas of the cortex may try and eventually succeed in replacing cortical motor systems which have been damaged, the brain must still have at its own disposal a corticofugal pathway for sending the motor output signals to the

spinal-muscular system. It seems unlikely to predict a good motor outcome if the integrity of the CST, especially of the ipsilesional one, has been heavily insulted.

To classify patients who can even be similar, at least in the first stages, according to a clinical assessment of their motor performances, identifying those whose CST is still intact, could not only predict the patients who will have a better recovery, but it could trigger some research about the rehabilitation therapies as well; it is not that improbable that patients, although similarly impaired by a clinical point of view, but with a different damage localization, or with a different degree of disruption of the CST, could benefit from different and personalized rehabilitative strategies.

Apart from conventional magnetic resonance imaging (MRI) and TMS, the integrity of the CST can be assessed through diffusion based probabilistic tractography, a relatively new MRI technique based on water diffusion.

This dissertation will focus on the preliminary results of a wider research project aimed to verify the reliability and usefulness of diffusion based probabilistic tractography of the corticospinal system as a predictive measure of the recovery potentialities of patients affected from stroke and suffering from a motor impairment.

The features, the investigations and the results carried on the patients and the controls during my research project will be preceded by an introduction on the principles and potentialities of diffusion based tractography. Being probable this technique will become a widespread clinical application, it is important, for clinical neurologist as well, to have an idea of its basic fundaments, and not

only of its futurable applications, but also of its limitations. I have attempted to write this introduction with the clinician in mind, assuming that the reader has only a passing familiarity with MRI.

Introduction to diffusion tensor imaging

Diffusion tensor imaging (DTI) can grant a unique view of tissue structure and organisation of the brain in vivo: it can measure the displacement of water molecules occurring between 10^{-8} and 10^{-4}m, according to a timescale ranging from few milliseconds to few seconds. In vivo, water diffusion is constrained by the presence of neurolemma, cellular membrane and cytoplasmatic organelles; this is the reason why its measurement mirrors the integrity of a tissue microstructure. For example, the white and grey matter are characterised by different diffusion measurements in normal conditions, which reflect their different structures. Conversely, the water diffusion measures change in pathological conditions, giving us precious clues when a brain is affected from several disorders at least, if not in all of them.

For a full understanding of DTI basic principles, few physics notions about water diffusion are needed.

The term Brownian motion, formally described by Albert Einstein in 1905, describes the displacement of free water molecules in a fluid consequent to thermal energy (16).

When the molecules move in a free space, their displacement is completely random, and it is limited by the container limits only. For example, if we shed an ink drop in a glass of water, we shall notice that progressively the spot of colour tends to expand, assuming the shape of a sphere, and that the diameter of this sphere will augment as the time goes by: at the very end, its expansion will be stopped as soon as it reaches the wall of the glass.

The speed with which free water molecules expand our ink sphere is influenced by their own size (mass), and the temperature and nature (viscosity) of the medium; describing their displacement distribution in a cartesian two-axis scheme, it will assume a Gaussian (bell-shaped) distribution. At 37℃, after a 50 msec diffusion time interval, 32% of the molecules will have moved at least 17 μm, whereas only 5% of them will have exceeded a 34 μm distance. The motion of these molecules is random and equal in all directions, this is defined as isotropic (see fig.1) (17).

Diffusion-weighted magnetic resonance imaging (DWMRI) exploits water molecule Brownian motion providing in vivo information related to microscopic structural features and geometric organization of neural tissues, both in physiological and pathological states.

Indeed, compared to the ones contained for example in a glass, water molecules in tissues cannot diffuse freely: as stated before, their motion is limited by the presence of cellular structures such as cell membranes, fibres and macromolecules. For this reason Brownian motion is often anisotropic in organisms (see figure 1) (18). Water diffusion can be detected with MRI through the use of a pair of sharp magnetic field gradient pulses, whose duration and separation can be adjusted: the first pulse magnetically 'labels' protons compounding the water molecules according to their spatial location; the second pulse is given slightly later to measure the positional variation of protons. If protons diffuse along the gradient direction, it will determine a change in the magnetic field "seen" by nuclei, to an extent that is proportional to

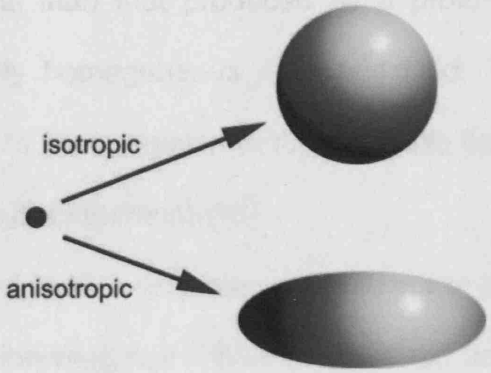

Figure1: in this picture the imaginary ink drop of our example shows two ways of diffusion: the one on the top shows the isotropic diffusion, in which the water displacements is equivalent in all directions; the one on the bottom shows an anisotropic diffusion, in which its displacement is not the same in all the directions.

the displacement of protons themselves; it results in an MRI radiowave signal slightly less powerful than that produced by a proton population conversely placed in a perfectly homogeneous magnetic field. The signal reduction is directly proportional to the extension of the magnetic field and, of course, to the degree of the proton displacement (18).

The images acquired in the presence of the diffusion sensitizing gradients are referred to as diffusion-weighted DWMRI. As stated above, the more a proton diffuses, the bigger is the signal attenuation, whilst, the less a proton diffuses, the less is the signal attenuation. The signal attenuation is influenced also by the degree of the magnetic field gradients, and the time during which the diffusion process takes place, that is actually the interval time between the two magnetic pulses. According to this, we can expect that signal transmitted by protons in free water, like the ones of the ventricular cerebrospinal fluid, in which the water diffusion degree is bigger, will appear hypointense; in contrast, nuclei bounded to water of tissues with a lower diffusion degree will show a more intense signal or appear hyperintense (see figure 2). As stated above, different region of the brain shows a different diffusion. However, some points should be borne in your mind:

- water diffusion is a three-dimensional process;
- neuronal tissue has a prevalently fibrillar organization, as a consequence of the fact that axons are mostly packed, coherently aligned in bundles;
- axons are surrounded by their myelin sheath and glial cells, that limit water diffusion perpendicularly to the main direction of the axon itself (see fig.3).

2A **2B** **2C**

Figure 2A: a normal DWMRI image; the signal coming from the lateral ventricles appears dark (deeply hypointense), whilst the one coming from the other structures of the brain will show different degrees of intensity related to the water diffusion present in that portion of the parenchyma.
Fig.2B and 2C: conventional T2-weighted (2B) and diffusion-weighted MRI (2C) of hyperacute infarction. The two images, acquired at the same time, show the superiority of DWMRI in detecting acute stroke early (hyperintensity of left basal ganglia in DWMRI). Cytotoxic oedema secondary to stroke is associated with less water diffusion than in healthy tissue, resulting in a hyperintense signal of the ischemic tissue.

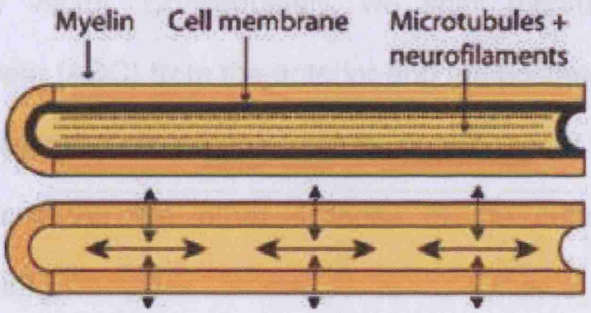

Figure 3: this scheme displays the major determinants of longitudinal water diffusion along the major direction of the axon, modified from (19).

This is the reason why various regions of the brain show not only a different degree of water diffusion, but also different preferential directions of water diffusion, secondary to the main orientation of the bundles of that area. In MRI this phenomenon is described through the so called diffusion tensor model.

Let's imagine we consider the brain as it were made up of a number of cube-shaped voxels and, in each of them, a single water molecule is positioned in the exact middle of the voxel itself. After recording the position of our water molecule at time 0, we wait for a short time (some milliseconds, actually), and then we shall measure from each of the 6 faces (anterior, posterior, caudal, rostral, right and left) of our cube-shaped voxel along which direction the water molecule diffused. For the sake of simplicity, we can suppose that, because of the microscopical structure of that voxel, our molecule moved only along an anterior-posterior vector. Consequently, we shall record a high Apparent Diffusion Coefficient (ADC) from the anterior and the posterior face of our cube-shaped voxel (displayed as a hyperintense signal), whilst a low ADC will be recorded from each of the other 4 faces of the cube (displayed as a hypointense signal).

ADC reflects the probability that water molecules have to diffuse along each of the 6 main directions of the space for every single voxel. So, each motion-probing gradient will give rise to a different image, according to the case if water diffusion was oriented toward the direction of the gradient itself. Different region of the brain shows a different diffusion values (see figure 4). Grouping the data coming from 7 images, one taken with b = 0 (no diffusion sensitivity), which works as a baseline, and the other 6 images (with diffusion gradients applied

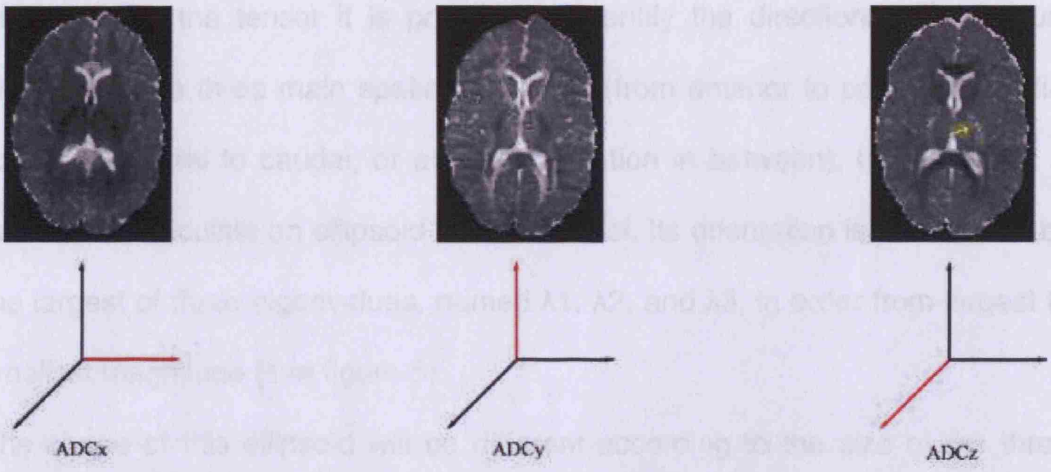

Figure 4: three transverse ADC maps of same brain slice with diffusion gradients applied in different directions: ADCx along the lateral-medial direction, ADCy along the anterior-posterior direction, and ADCz along the rostral-caudal direction. A different anisotropic diffusion is detected in each single figure: signal intensity of white matter varies with direction of diffusion gradients, most conspicuously in corticospinal tracts: signal is strongest when diffusion gradient is oriented orthogonally to white matter fibres tracts, as indicated by the yellow arrow in the third image.

along six unique directions), that allow the calculation of the water diffusion tensor. From the tensor it is possible to identify the directions of maximum diffusion in the three main spatial directions (from anterior to posterior, medial to lateral, rostral to caudal, or at any orientation in between), from which it is possible to calculate an ellipsoid for each voxel. Its orientation is determined by the largest of three eigenvalues, named λ1, λ2, and λ3, in order from largest to smallest magnitude (see figure 5).

The shape of this ellipsoid will be different according to the size of the three eigenvalues: if water displacement is equal in all the directions, $\lambda 1 = \lambda 2 = \lambda 3$, it means water has isotropic diffusion, and the resulting ellipsoid will assume a spherical shape (see figure 6). However, if $\lambda 1 > \lambda 2 = \lambda 3$, water has an anisotropic diffusion, and the resulting ellipsoid will assume a cigar-like shape (see figure 6).

Up to this point, a diagonalized tensor matrix was calculated for each single voxel. As stated above, at least 6 measurements are required, but a larger number would render these calculations much more precise: diffusion measurements obtained in 126 directions have been published (20).

A tridimensionally oriented ellipsoid will be present in each voxel, and their shapes and orientations will reflect the main water diffusion directions. As we can see in fig. 7, their orientation will be modulated by the main bundles of the brain. A further analysis of these data will allow us to trace single bundles. A common technique is to calculate the probability of connection between two points, choosing two regions of interest (ROI). For example, to identify the

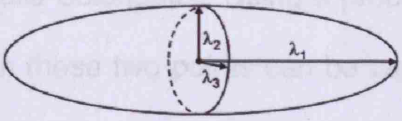

Figure 5: graphical representation of an ellipsoid derived from three major eigenvectors, named λ1, λ2, and λ3. In this case, λ1 is prominent compared to λ2 and λ3.

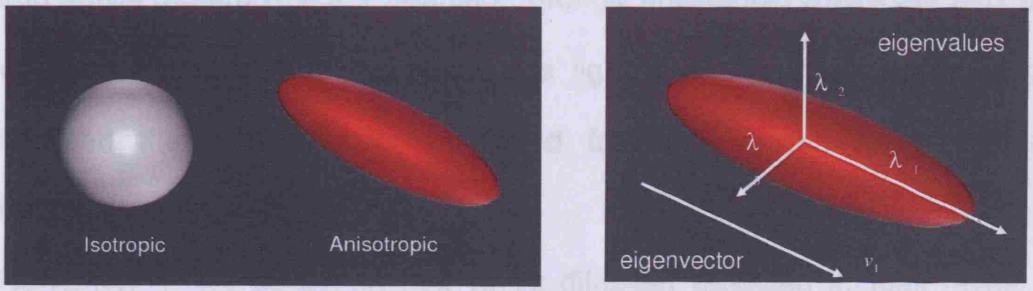

Figure 6: the value of if λ1, λ2 and λ3 will determine a different shape of the ellipsoid.

Figure 7: this figure shows an orientation distribution function map of a coronal brain section. A color scale is used (blue for rostral-caudal orientation, red for latero-lateral orientation, and green for anterior-posterior orientation). The biggest white matter bundles, such as the corticospinal tract and the Corpus Callosum can be easily identified. From (20).

corticospinal tract, one may choose two ROIs (e.g. internal capsule and the ventral surface of medulla oblongata). Using a probabilistic algorithm, the most probable route between these two points can be calculated. In order to explain this process, in figure 8a a certain number of voxels (with each their own eigenvector inside) are represented in a bidimensional grid. A departure (red) and arrival (green) ROI are selected. Strongly anisotropic voxels are dark blue, whereas weakly anisotropic voxels are light blue. The most probable route between the two ROIs is calculated following voxel-to-voxel directional information (figure 8b).

Generally, it can be stated that whilst diffusion weighted images reveal the distance covered in a certain time by the water molecules, the diffusion tensor gives us information not only about the degree of diffusion, but also about the direction of water diffusion. In other words, each voxel will not be represented anymore by a hyper or a hypointense signal, but by a tensor from which we can identify the principal eigenvector, and whose orientation will reflect the main direction of water diffusion. This will reflect the main axonal orientation in each single voxel, allowing us to detect the hodology and/or verify the integrity of a single bundle.

Since the tensor model is unable to resolve crossing fibres, methods have been developed to address this challenge (20). Currently, tractography plays a pivotal role in anatomical and neuroscience research (21). However it is not a widespread clinical application yet, several applications evolving over the near future may be envisaged, such as in spinal

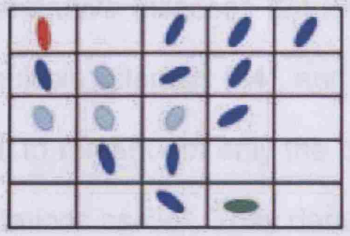

8A

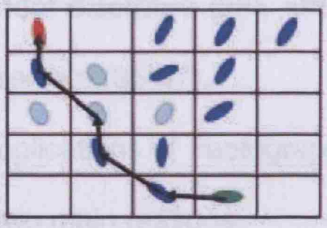

8B

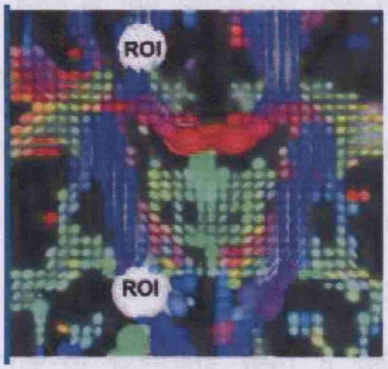

8C

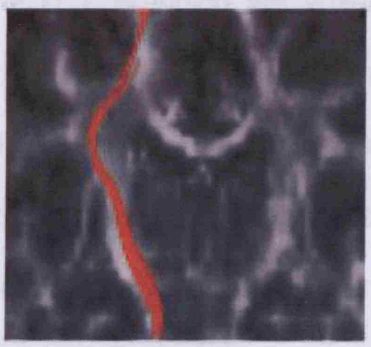

8D

Figure 8A: bidimensional representation of a group of voxels containing inside with each their own eigenvector inside.
Figure 8B: the most probable route between the start (red) and arrival (green) ROIs was calculated.
Figure 8C and 8D: the same concept is displayed in 3D images.

cord injury (22, 23), early and/or differential diagnosis in several neurodegenerative diseases (24-27), child development disorders (28), stroke (29-33), multiple sclerosis (34), and presurgical assessment (35-37).

It is pivotal to remark not only the possible clinical applications of tractography, but its limitations as well. They derive basically from two main reasons.

The first one is the relatively low resolution of the DTI, in which the voxels dimensions typically range from 2 to 3 mm; on the other hand, the axons diameter is around 1μm. That means that the diffusion of water molecules displacing inside contiguous axons is averaged and assessed in a much bigger voxel, so that several bias can take place when a single voxel contains different populations of bundles with a different spatial orientation. This happens especially when a voxel contains "crossing" or "kissing" fibres: usually it is not possible for diffusion tensor imaging to distinguish between these two situations. The limits of diffusion tensor imaging voxel dimension intervene also when dealing with bundles with a very short curvature radius. It is the case of the sub-cortical U-fibres, which are that convoluted to be contained inside a single voxel space (38)

The second main reason is the noise contained in diffusion tensor imaging acquisitions, which can mislead a correct evaluation of the real axonal orientation, determining an apparent deviation. Concluding, this bias must be kept in mind when interpreting the results of tractography (39).

Aims and hypotheses of the present study

The aims of this study are:

- To quantify the integrity of the corticospinal bundle as assessed by probabilistic tractography in patients who suffered from stroke;
- To investigate whether the integrity of the corticospinal bundle, as assessed by probabilistic tractography, correlates with: (i) the cortical-spinal system integrity as assessed by TMS, (ii) the degree of motor impairment and/or (iii) the degree of functional improvement achieved by the patients during a two week period of intensive upper limb training.

The target of our analysis is to calculate the FA of the CST, choosing as ROIs the primary motor cortex areas (precentral gyrus and central sulcus) and the cerebral peduncles. Computing will be performed through a probabilistic tractography algorithm.

Since connectivity is compromised from the disruption of the fibres, it is reasonable to expect that our patients, who suffered from stroke with various degrees of hemiparetic symptoms, will show a lower value of affected hemisphere CST FA compared to controls.

Furthermore, we shall test whether our measures of connectivity correlate with disability, assessed by 5 clinical and neurophysiological scales:

1. Action Research Arm Test or ARAT;
2. 9-Hole Peg Test or 9HPT;
3. Jebsen-Taylor Hand Function Test or JTT;
4. Maximum grip strength test or GRIP;

5. TMS.

TMS is a noninvasive method to determine the activation of the cortical neurons. Neuronal activity can be triggered by rapidly changing magnetic fields, determining the excitement of the brain neurons.

A coil of wire, encased in plastic, is held proximally to the head, in a position corresponding to the cortical region which is targeted. A large capacitor energizes the coil through a rapidly changing current, producing a magnetic field which orientation is orthogonal to the plane of the coil. This will induce weak electric currents in cerebral tissue, giving rise to the activation of the nerons. The discomfort given to the tested subject is minimal.

TMS is a widely-accepted way to measure the connection between the motor cortex and the muscles. Clinically, it is most useful in disorders such as stroke, multiple sclerosis, motor neurons degenerative disorders and spinal cord injury. When applied on the motor cortex, TMS gives rise to MEPs, which can be recorded peripherically, and which are, in normal subjects, proportional to the intensity of the stimulation applied to the motor cortex. The proportionality of this curve can be recognized between TMS intensity values ranging from the lowest one, capable to give rise to a recordable MEP, to the highest capable to evoke the maximum contraction in the peripherial muscle. The profile of this curve is one of the parameters commonly accepted for verifying the functional integrity of CST. Further details will be given in the methods section.

The existence of a significant correlation between affected side CST disruption assessed through probabilistic tractography, motor disability (assessed by the clinical scales) and/or TMS would support the use of CST probabilistic

tractography as an outcome measure for the assessment and the recovery prediction of patients affected from stroke.

Methods

Subjects

Patients were recruited from the outpatients clinics of the National Hospital for Neurology and Neurosurgery, London. All of them suffered from their first-ever stroke at least one year before the acquisition of the DTI images.

In all patients weakness of at least wrist and finger extensors and hand interossei (with a score equal or minor to 4, according to the Medical Research Council Scale) was present for at least 48 hours after the onset of the symptomatology.

Patients were excluded in case of:

- Involvement of the primary motor cortex and/or the brainstem in infarcted brain tissue;
- Cognitive or language impairment able to deny a full cooperation during the study;
- Complete paresis of the hand grip;
- Occurrence of any previous seizure;
- Record of any neurological motor disability before the cerebrovascular event.

A two weeks intensive physiotherapy treatment of the upper limb was also given as part of a separate clinical trial. Imaging data were acquired prior to the treatment period. Neurophysiological data and motor impairment scores were acquired immediately before and after the treatment period.

An age matched control group, compounded by healthy subjects, without any history of neurological or psychiatric history and not taking any regular medication. The study was approved by the Joint Medical Ethics Committee of the National Hospital for Neurology and Neurosurgery and the Institute of Neurology, London. All subjects were asked to sign a written informed consent before the study.

MRI acquisition

All the controls and the patients were scanned in the Wellcome Trust Centre for Neuroimaging, Institute of Neurology, University College London. We acquired DWI on a 3.0 T Allegra Scanner (Siemens, Erlangen, Germany). DWI was performed with an echo planar sequence comprising a double spin-echo module to reduce the effect of eddy currents (40). Data acquisition was cardiac gated to reduce motion artefacts from cerebrospinal fluid pulsation (41). Each data volume consisted of 40 axial slices of 2.3 mm thickness with no inter-slice gaps and an acquisition matrix of 96 x 96 in a field of view of 220 x 220 mm, resulting in 2.3 × 2.3 × 2.3 mm^3 isotropic voxels (TE=90 ms, flip angle 90 degrees, fat saturation, bandwidth 2003 Hz/Pixel). Each data set consisted of 61 high diffusion-weighted images (b = 1000 s/mm2), with diffusion gradients applied along 61 evenly distributed diffusion directions obtained from a previously reported optimisation procedure (42) and 7 additional images with minimal diffusion-weighting (b = 100 s/mm^2) and evenly distributed directions. The diffusion tensor was fitted using a standard linear least squares fit to the log measurements (43). Additionally, the fitting provides an effective b = 0 image. From each subject we also acquired high-resolution T1 weighted structural data using the MDEFT sequence (176 slices, 1 mm thickness, sagittal, phase encoding in anterior/posterior, FoV 224 x 256 mm, matrix 224 x 256, TR=20.66 ms, TE=8.42 ms, TI=640 ms, flip angle 25 degrees, fat saturation, bandwidth 178 Hz/Pixel) (44).

Images analysis

Normal T1 images and diffusion tensor images were processed using different software tools, and in different steps as follow and as illustrated in figure 8.

Data processing

I first describe the creation of seed and target maps in subject-specific native space using Freesurfer (http://surfer.nmr.mgh.harvard.edu), a freely available software for automated segmentation and structure labelling (45). This is followed by a description of the fibre tracking algorithm, the generation of spatial transforms and finally, the statistical analysis.

Preparation of seed and target areas

In order to allow bias-free definition of seed and target areas unaffected by subjective judgements about anatomical correspondences we performed automated cortical and sub-cortical segmentation and labelling in subject-specific native space.

Using MRICron (http://www.sph.sc.edu/comd/rorden/mricron) we defined manually the extent of the left cerebral peduncle in the axial plane on a T1 weighted image in standardised MNI (Montreal Neurological Institute) space.

In order to avoid differences in the number of seed voxels we flipped the left ROI to the opposite side and defined this as the right cerebral peduncle. Freesurfer's output consists of forty-six automatically labelled cortical areas covering the whole cortex. We defined both the automatically labelled left

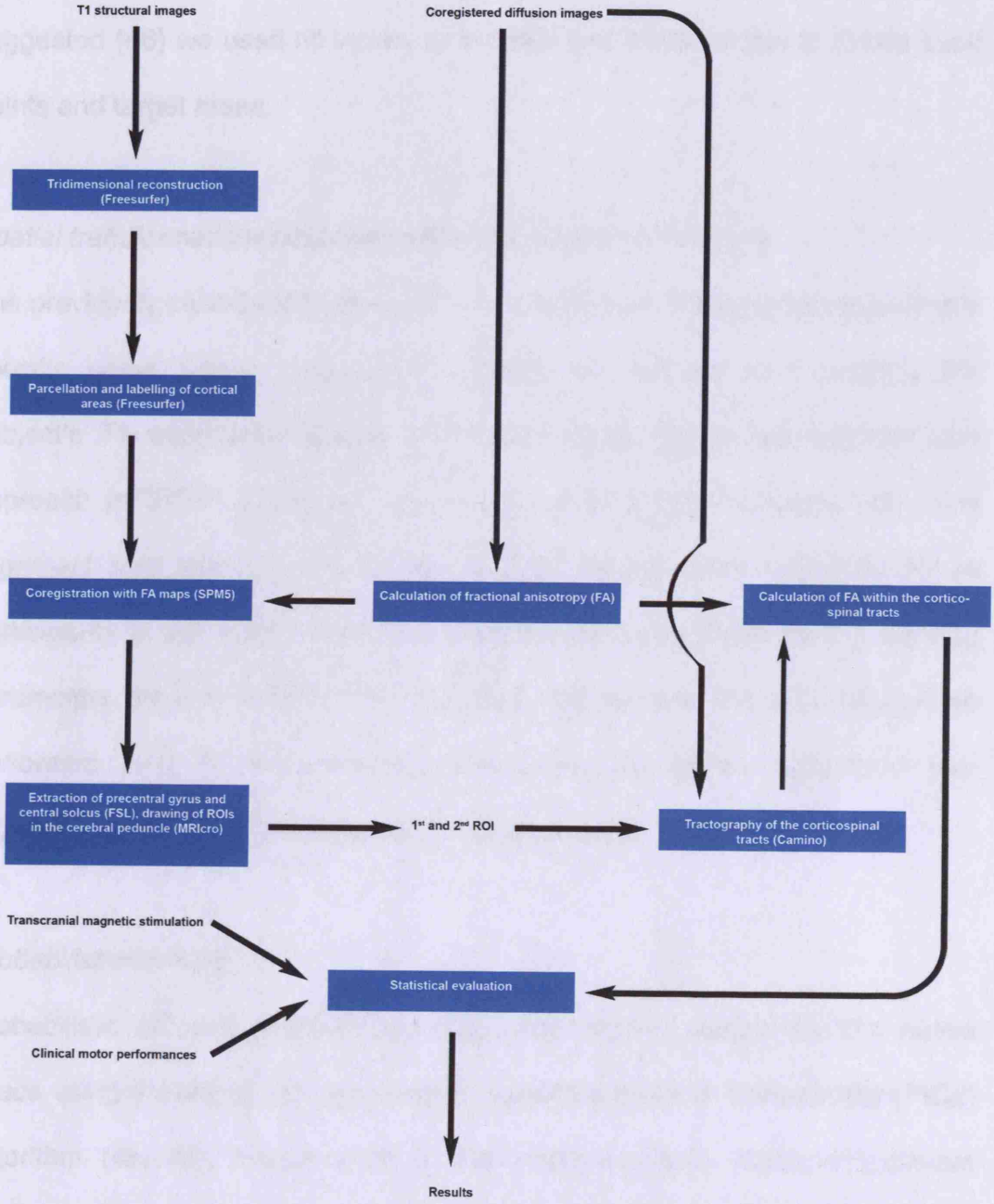

Figure 9: Flowchart of images processing and analysis.

and right motor cortex as targets for probabilistic tracking. As previously suggested (46) we used all voxels in the ROI and motor cortex to define seed points and target areas.

Spatial transformations between native and standardised space

The previously described ROIs were transformed from standardised to subject's specific native space using spatial transforms derived from warping the subject's T1 weighted image in MNI space using the unified segmentation approach in SPM5 (http://www.fil.ion.ucl.ac.uk/spm/software/spm5) (47). The alignment after spatial transformation was proven by visual inspection for all participants in the study. To reassure correspondence between the warping parameters derived from the T1 weighted images and the DTI dataset we performed prior to the tracking experiments an affine registration (co-registration) between these datasets for each subject.

Probabilistic tracking

Probabilistic diffusion tractography was performed in subject-specific native space using the previously described Probabilistic Index of Connectivity (PICo) algorithm (48, 49), implemented in the freely available "Camino" software package (http://www.cs.ucl.ac.uk/research/medic/camino) (50). PICo involves repeated iterations of a streamline process using Monte Carlo methods to model inherent uncertainty in the orientation of the principal diffusion direction(s) defined for each voxel. First, we identified fibre crossings using the algorithm proposed by Alexander *et al* (51) and parameterised them with a

mixture of two tensors (52); in all other parenchymal voxels a single tensor model was used. We then applied the method of Cook *et al.* (53) to compute probability density functions (PDFs) of the fibre tract orientation estimated from the principal direction of each diffusion tensor(s) in each voxel, under the assumption that dominant orientations derived from the diffusion-weighted data correspond to the dominant orientations of fibre bundles. Stopping criteria prevented biologically implausible curvature of streamlines (> 180°on the scale of a single voxel) or attempts to transit voxels with FA value less than 0.1. Five thousand iterations were used to identify each connection route. Each seed point, its co-ordinate and probability of connection to a given target area were used for further analysis. PICo is derived as the proportion of the total number of samples from a seed voxel that reach a target area. Additionally, we calculated on a voxel-by-voxel basis, using "Camino" software, fractional FA maps based on the three eigenvalues of each diffusion tensor (54, 55).

FA estimation in the CST

Based on the probabilistic tracking output we created binary images of the pathways connecting the ROI in the cerebral peduncle and the ipsilateral motor cortex. The pathways represent either the mean or the maximum probability map of connection between a single seed voxel and the whole target region. For the extent of these pathways we extracted the corresponding mean FA values from each subject's FA map. Additionally, we applied a PICo threshold of 0.01 on both the mean and maximum connectivity maps. The 0.01 threshold was chosen, after several trials, as the lowest value that excluded those 'outlier'

voxels. These results entered the statistical analysis.

Clinical and neurophysiological assessment

The 9HPT

The 9HPT is a test aimed to measure the dexterity of a patient: it requires a coordinated reaching and precision grip. Age and hand dominance influence the results. The advantage of this test is the simplicity, the reliability, the reproducibility and the relative investigator independence (56). A plastic box containing nine empty holes and a small, shallow container holding nine pegs is given to the patient, who is asked to pick up the nine pegs one at a time with one hand as fast as he can, to put them in the nine holes and, once there, to remove them again as quickly as possible one per time, replacing them into the shallow container (see figure 10). The total time normally needed for completing the test is 10–15 seconds.

Our patients have been assessed twice, before and after the two weeks treatment of upper limb intensive physiotherapy was given. Both upper limbs were assessed. The score was expressed as a ratio, given by time in seconds of the affected hand/time in seconds of the healthy hand.

Controls were not assessed through 9HPT.

ARAT

The ARAT is a reliable and valid measure of arm motor capabilities after stroke. First described by Lyle (57), it has an established value for characterizing clinical state and for the assessment of the spontaneous and therapy-induced recovery. A paper suggesting a standardized approach, not only for the evaluation and scoring of the patient performances, but also for

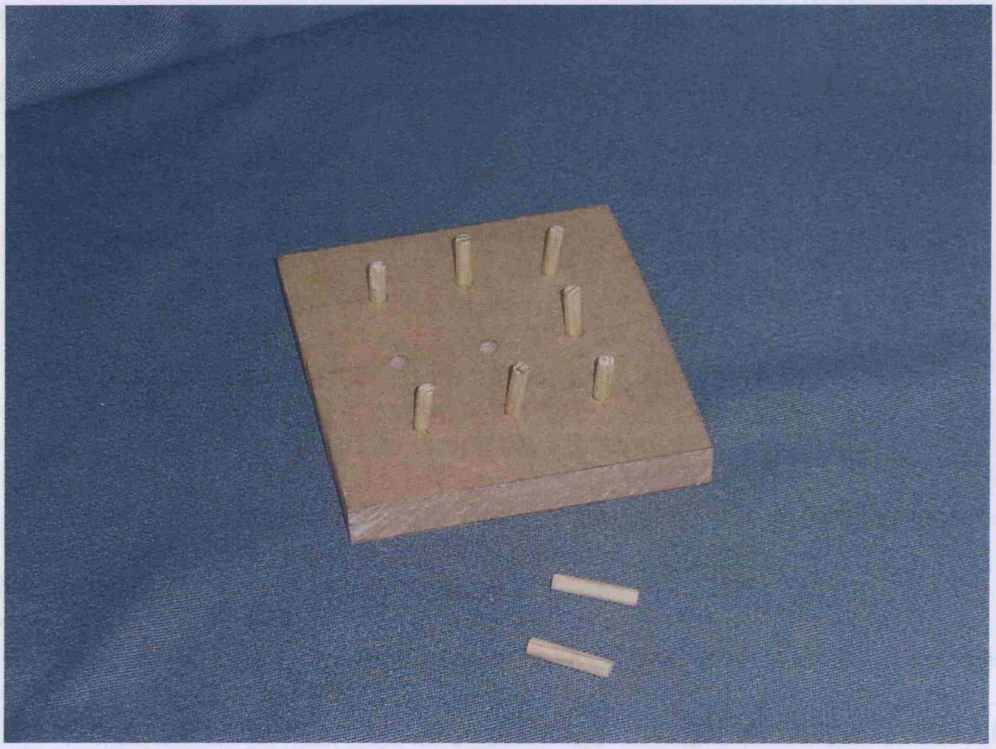

Figure 10: 9-Hole Peg Test

the choice and displacement of the tools during the different tasks, was recently published (58).

When performed in a standardized manner, ARAT is considered a useful tool for assessment of arm motor deficits after stroke.

It consists of 4 subscales:

- grasp subscale, consisting of 6 tasks
- grip subscale, consisting of 4 tasks
- pinch subscale, consisting of 6 tasks
- gross movement subscale, consisting 3 tasks

For each task, a score from 0 to 3 can be given, so the maximum score for each arm can arrive up to 57 (see figure 11).

Our patients have been assessed twice, before and after that the two weeks treatment of upper limb intensive physiotherapy was given. Only affected hand score was recorded.

Controls were not assessed through ARAT.

Test Number	Item	Score	
	Grasp subscale	Left	Right
1	Block, 10 cm'	0 1 2 3	0 1 2 3
2	Block, 2.5 cm'	0 1 2 3	0 1 2 3
3	Block, 5 cm'	0 1 2 3	0 1 2 3
4	Block, 7.5 cm'	0 1 2 3	0 1 2 3
5	Cricket ball	0 1 2 3	0 1 2 3
6	Sharpening stone	0 1 2 3	0 1 2 3
		Subtotal ____/18	____/18
	Grip subscale		
7	Pour water from one glass to another	0 1 2 3	0 1 2 3
8	Displace 2.25-cm alloy tube from one side of table to the other	0 1 2 3	0 1 2 3
9	Displace 1-cm alloy tube from one side of table to the other	0 1 2 3	0 1 2 3
10	Put washer over bolt	0 1 2 3	0 1 2 3
		Subtotal ____/12	____/12
	Pinch subscale		
11	Ball bearing, held between ring finger and thumb	0 1 2 3	0 1 2 3
12	Marble, held between index finger and thumb	0 1 2 3	0 1 2 3
13	Ball bearing, held between middle finger and thumb	0 1 2 3	0 1 2 3
14	Ball bearing, held between index finger and thumb	0 1 2 3	0 1 2 3
15	Marble, held between ring finger and thumb	0 1 2 3	0 1 2 3
16	Marble, held between middle finger and thumb	0 1 2 3	0 1 2 3
		Subtotal ____/18	____/18
	Gross movement subscale		
17	Hand to behind the head	0 1 2 3	0 1 2 3
18	Hand to top of head	0 1 2 3	0 1 2 3
19	Hand to mouth	0 1 2 3	0 1 2 3
		Subtotal ____/18	____/9
		Total ____/57	____/57

Figure 11: score scale for ARAT

JTT

JTT is a test widely used by physicians and occupational therapists as a broad measure of hand function. Its validity and reliability was proven in several clinical trials. Moreover, normative data for age and gender are available (59).

JTT in compounded by 7 subtests. In our study we included 6 of them;

- Turning over cards;
- Picking up small objects and placing them in a can;
- Picking up small objects with a teaspoon and placing them in a can;
- Stacking chequers;
- Moving large light cans;
- Moving heavy cans.

Our patients have been assessed twice, before and after that the two weeks treatment of upper limb intensive physiotherapy was given. Before starting the JTT, patients were asked to perform all the tests the quicker and the more precisely as possible (60). Only the affected hand was assessed, and the total time was recorded. No time penalty was given in case of "dropping" of an object.

Controls were not assessed through JTT.

GRIP

Maximum grip strength with each hand was measured for each patient using a Jamar hydraulic hand dynamometer (Fabrication Enterprises, Inc., NY, USA). Patients were seated with the elbow flexed at 90 degrees. They were asked to grip the dynamometer as hard as possible 3 times in a row. The maximum

value was recorded. The maximum voluntary contraction (MCV), expressed in Newton, was recorded.

This test was performed before and after the two weeks physiotherapy treatment. This method has been used previously (14).

Controls were not assessed through GRIP.

TMS

Subjects were seated comfortably in an arm chair with their eyes open. EMGs were recorded via Ag/AgCl electrodes, which were placed over the First Dorsal Intersosseus (FDI), of both the affected and the unaffected hands, using a belly-tendon montage. Signals were filtered (30Hz-10KHz) and amplified using a Digitimer 360 (Digitimer Ltd., Welwyn Garden City, Herts., UK) and then stored on computer via a Power 1401 data acquisition interface (Cambridge Electronic Design Ltd, Cambridge UK).

Measures were performed on 2 time points. Baseline measures were taken 10 days before the onset of the 2-week treatment period (two consecutive weeks Monday – Friday). The outcome measures were performed 4 days after the end of the treatment protocol, on the same time of the day as the baseline measures.

A hand held figure of eight coil connected to a monophasic Magstim *200* stimulator was used for the experiment (all Magstim Co., UK). The motor hot spot was initially identified on both sides of the brain; this was defined as the location on the scalp where TMS consistently resulted in the largest MEP. Once found a surface marking was made on the scalp to ensure positioning of the coil remained constant.

For the TMS measures, subjects were asked to maintain a steady background contraction of the affected FDI of 10% - 15% of maximum voluntary contraction (MVC). Visual feedback was given using an oscilloscope.

The following TMS measures were performed:

- Active Motor Thresholds (AMT): these were calculated for the ipsilesional during active contraction of the affected FDI. The AMT was defined as the lowest TMS intensity which evoked in 5 out of 10 trials an EMG response of about 200mV, or a response that was clearly distinguishable from the background EMG activity.
- Recruitment curve during background contraction (active RC): this measure was performed on the ipsilesional side using the same 70mm coil. 10 MEPs were collected while the subjects maintained a background FDI contraction of 15-20% of MVC at the following stimulus intensities: 110%, 130%, 140% and 150% AMT. Trials with excess or inadequate background contraction were rejected on-line.

Analysis of data was carried out using Signal Software (Cambridge Electronic Design).

For the active RC all the frames were visually re-inspected off line. The pre-stimulus EMG was averaged and trials falling outside the range of 3 standard deviations of the mean were rejected. The amplitude of the active MEP was defined as the peak-to-peak amplitude of the unrectified EMG activity recorded 20-100 ms after the TMS stimulus.

Amplitude measures for each intensity were then averaged and plotted against the TMS intensity. The slope of the resulting curve (Aslope) was calculated using a linear regression model (SPSS v.14; SPSS Inc., USA). For the linear model: MEP=Y+slope*I, where Y is the Y-axis intercept, I is the stimulation intensity. The maximal MEP amplitude recorded during the acquisition of the RC (MAX) was also noted. Controls were not assessed through TMS.

Statistical analysis

Computing was performed with SPSS 14.0. Statistical significance is taken at $P<0.05$.

Difference in CST FA between patients and controls

A statistical analysis was performed for comparing;

- The affected and the unaffected CST FA value among the patients;
- The affected CST FA value in patient and the mean CST FA value in controls;
- The unaffected CST FA value in patients and the mean CST FA value in controls;
- The ratio of affected CST FA value/unaffected CST FA in patients and the ratio of left CST FA value/right CST FA value in controls.

Since we meant to compare the value of a continuous variable (FA) in between different groups (affected CST in patients versus CST of controls, unaffected CST of patients versus CST of controls, CST ratio in patients versus CST ratio in controls), and because of the fact that our FA value do not have a normal distribution, as verified through the Shapiro-Wilk test, we used the Mann-Whitney U Test.

Correlations of CST FA with clinical and neurophysiological scores

A statistical analysis was performed for verifying the existence of any correlation between CST FA value in patients and ARAT, 9HPT, JTT, GRIP, and TMS measures.

Since we meant to compare the values of continuous variables (FA and clinical-neurophysiological values) among the patients group, and since these variables do not have a normal distribution, we used the Spearman Test.

Results

Patients

10 patients, with an average age of 56.4 years (range 40-77 years, standard deviation ±12.5), 4 males and 6 females, were recruited. None of the patients had infarction involving primary motor cortex or brainstem, as assessed on T1 weighted images (see figure 12). The clinical features of the patients are summarized in table 1.

We also enrolled 9 normal controls with an average age of 52.3 years (range 21-76 years, standard deviation ±19.12), 6 males and 3 females.

Clinical and neurophysiological assessment

The patients' assessment data acquired before (T0) and after (T1) the two weeks of rehabilitative treatment are shown in table 2 for 9HPT, ARAT and JTT, and in table 3 for GRIP, Aslope and MAX.

The scores achieved by the patients in the 9HPT are expressed with the ratio (time in seconds in the affected hand/time in seconds in the healthy hand).

The numbers showed for the ARAT correspond to the raw score achieved by the patients.

The scores achieved by the patients in JTT are expressed in seconds needed by the patient himself for performing all the tasks of our modified JTT. Patient 6 was not able to perform the test during the basal assessment.

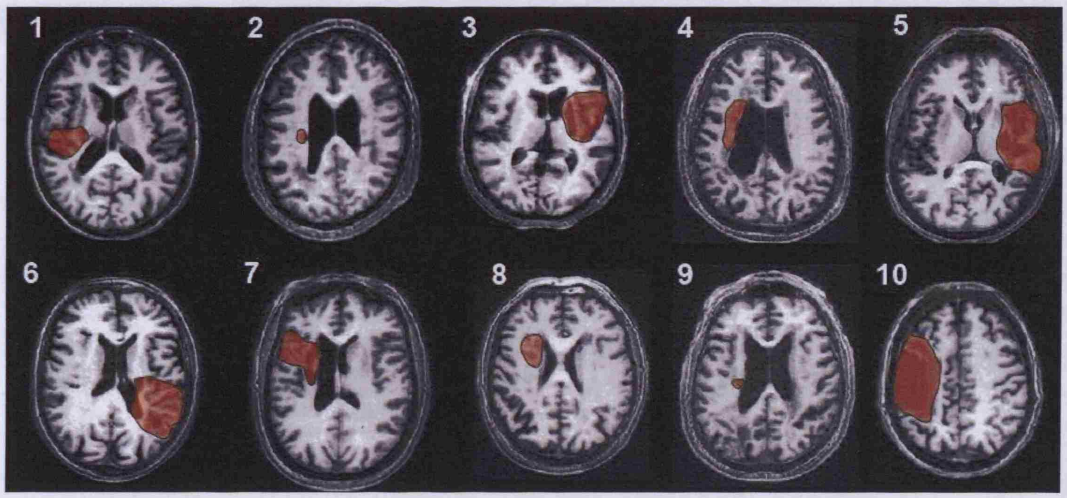

Figure 12: T1 weighted axial images showing the lesion site in each of our patients.

	Site of the lesion	Age	Gender	Affected hemisphere	Months from stroke
Patient 1	internal capsule (posterior limb)	77	Female	Dominant	26
Patient 2	corona radiata	51	Male	Non dominant	60
Patient 3	striatocapsular	45	Female	Non dominant	29
Patient 4	corona radiata	66	Male	Dominant	26
Patient 5	posterior branch middle cerebral artery	46	Female	Non dominant	25
Patient 6	posterior branch middle cerebral artery	60	Female	Non dominant	288
Patient 7	middle branch middle cerebral artery	40	Female	Dominant	20
Patient 8	corona radiata	53	Male	Dominant	13
Patient 9	corona radiata	74	Male	Non dominant	26
Patient 10	middle cerebral artery	52	Female	Dominant	84

Table 1: Features of patients.

	9HPT T0	9HPT T1	ARAT T0	ARAT T1	JTT T0	JTT T1
Patient 1	0.018	0.044	19.5	21	124.858	155.213
Patient 2	0.327	0.352	48	50	102.107	112.204
Patient 3	0.066	0.224	34	41	136.235	78.406
Patient 4	0.439	0.468	38	48	74.253	82.056
Patient 5	0.364	0.313	55	56	117.006	80.266
Patient 6	0.000	0.042	19.5	32	Unable to do anything	260.078
Patient 7	0.355	0.548	54	57	62.756	49.976
Patient 8	0.588	0.623	49	57	60.5166	55.446
Patient 9	0.369	0.435	47.5	55	67.0733	51.2066
Patient 10	0.036	0.106	32	34	147.595	118.07

Table 2: Score achieved by patients before (T0) and after (T1) the rehabilitation treatment. HPT is expressed trough the ratio time in seconds in the affected hand/time in seconds in the healthy hand; ARAT is expressed though the raw score; JTT is expressed through the number of seconds needed by the patients for performing it.

	GRIP T0	GRIP T1	Aslope T0	Aslope T1	MAX T0	MAX T1
Patient 1	114.66	114.66	0.006	0.006	0.594	0.509
Patient 2	117.79	122.28	0.001	0.004	0.436	0.503
Patient 3	80.72	103.57	-	-	0	0
Patient 4	233.93	252.73	0.02	0.034	1.682	1.733
Patient 5	107.80	147	0.016	0.011	1.005	0.755
Patient 6	73.64	73.82	-	-	0	0
Patient 7	219.49	242.96	0.007	0.005	0.400	0.522
Patient 8	204.51	218.20	0.009	0.016	0.519	0.829
Patient 9	188.80	286.15	0.031	0.018	1.986	1.299
Patient 10	97.72	92.98	-	-	0	0

Table 3: Score achieved by patients before (T0) and after (T1) the rehabilitation treatment. GRIP is expressed the Newton exerted by the patient's affected hand through the manipulandum. Aslope is the slope of the RC during TMS. MAX is the MEP intensity in mV.

The numbers shown in the GRIP table columns represent the strength (measured in Newton) exerted with the affected hand by the patient with the manipulandum.

The numbers shown in the Aslope columns represents the slope coefficient of RC. The numbers shown in the MAX colums is the intensity in mV of the maximal MEP amplitude recorded during the acquisition of the RC. No MEP could be recorded from patient 3, 6 and 10 during TMS assessment.

FA anisotropy of CST

The values of mean CST FA were extracted in both hemispheres in patients (affected and unaffected side) and controls (right and left). FA values were extracted from the unthresholded and thresholded mean connectivity maps (MeanC and TMeanC), and from the unthresholded and thresholded maximum connectivity maps (MaxC and TMaxC). Results are shown in table 4 for patients and table 5 for controls

	Affected TMeanC	Unaffected TMeanC	Affected MeanC	Unaffected MeanC	Affected TMaxC	Unaffected TMaxC	Affected MaxC	Unaffected MaxC
Patient 1	0.3532	0.3339	0.3441	0.4251	0.3441	0.3747	0.3441	0.3339
Patient 2	0.4289	0.4233	0.3942	0.4888	0.4184	0.4431	0.3942	0.4233
Patient 3	0.3858	0.471	0.4077	0.3943	0.4003	0.4213	0.3858	0.3943
Patient 4	0.348	0.3709	0.3069	0.4627	0.3149	0.4046	0.3069	0.3709
Patient 5	0.4357	0.4958	0.4816	0.4185	0.4371	0.4599	0.4357	0.4185
Patient 6	0.3746	0.466	0.4117	0.362	0.3839	0.4154	0.3746	0.362
Patient 7	0.4503	0.4114	0.388	0.4781	0.4307	0.4274	0.388	0.4114
Patient 8	0.3633	0.3513	0.3152	0.4319	0.3302	0.3513	0.3152	0.3513
Patient 9	0.3951	0.3392	0.3312	0.4477	0.3312	0.3552	0.3312	0.3392
Patient 10	0.4645	0.4059	0.3933	0.4882	0.4267	0.4414	0.3933	0.4059

Table 4: CST FA values in the affected and unaffected side of patients

	Left TMeanC	Right TMeanC	Left MeanC	Right MeanC	Left TMaxC	Right TMaxC	Left MaxC	Right MaxC
Control 1	0.5107	0.5258	0.4131	0.388	0.4741	0.4248	0.4131	0.388
Control 2	0.4667	0.4614	0.4025	0.3953	0.4382	0.4374	0.4025	0.3953
Control 3	0.489	0.4854	0.4143	0.3811	0.4492	0.4305	0.4143	0.3811
Control 4	0.5066	0.5039	0.4169	0.3935	0.4458	0.4114	0.4169	0.3935
Control 5	0.4852	0.498	0.3749	0.3718	0.4213	0.4166	0.3749	0.3718
Control 6	0.4589	0.4575	0.3604	0.365	0.4155	0.4101	0.3604	0.365
Control 7	0.46	0.4967	0.3794	0.3865	0.4124	0.4401	0.3794	0.3865
Control 8	0.4549	0.4421	0.3588	0.3866	0.4162	0.4092	0.3588	0.3866
Control 9	0.5029	0.4972	0.4118	0.4227	0.4363	0.4545	0.4118	0.4227

Table 5: CST FA values in the left and right side of controls.

Difference between affected and unaffected CST FA of patients

We found a significant difference between the affected and the unaffected CST of patients in the values of FA calculated on TMeanCs (see table 6).

Difference between left and right CST FA of controls

We did not find any significant difference between the left and the right controls' CSTs in the values of FA calculated on TMeanCs, TMaxCs, MeanCs and MaxCs (see table 7).

Difference between affected CST FA of patients and bilateral mean CST FA of controls

We found a significant difference between the affected CST of patients and the bilateral mean CST FA of controls calculated on TMeanCs and TMaxCs, but not on those calculated on the MeanCs and MaxCs (see table 8).

Difference between unaffected CST FA of patients and bilateral mean CST FA of controls

We did not find a significant difference between the unaffected CST of patients and the bilateral mean CST of controls in the values of FA calculated on TMeanCs, TMaxCs, MeanCs and MaxCs (see table 9).

Difference between affected side CST FA / unaffected side CST FA of patients and left CST FA value/right CST FA value in controls

We found a significant difference between the affected side CST FA / unaffected side CST FA of patients and left CST FA value/right CST FA value in controls in the values of FA calculated on TMeanCs and TMaxCs, but not on the values of FA calculated on the MeanCs and MaxCs (see table 10).

	TMeanC FA	MeanC FA	TMaxC FA	MaxC FA
Mann-Whitney U	15.000	37.000	31.000	37.000
Wilcoxon W	70.000	92.000	86.000	92.000
Z	-2.646	-.983	-1.436	-.983
Asymp. Sig. (2-tailed)	.008	.326	.151	.326

Table 6: Mann-Whitney U Test between the affected and the unaffected CST FA of patients.

	TMeanC FA	MeanC FA	TMaxC FA	MaxC FA
Mann-Whitney U	38.000	37.000	30.000	37.000
Wilcoxon W	83.000	82.000	75.000	82.000
Z	-.221	-.309	-.927	-.309
Asymp. Sig. (2-tailed)	.825	.757	.354	.757

Table 7: Mann-Whitney U Test between the left and the right CST FA of controls.

	TMeanC FA	MeanC FA	TMaxC FA	MaxC FA
Mann-Whitney U	8.000	28.000	16.000	28.000
Wilcoxon W	63.000	83.000	71.000	83.000
Z	-3.021	-1.388	-2.368	-1.388
Asymp. Sig. (2-tailed)	.003	.165	.018	.165

Table 8: Mann-Whitney U Test between the affected CST FA of patients and bilateral mean CST FA of controls.

	TMeanC FA	MeanC FA	TMaxC FA	MaxC FA
Mann-Whitney U	27.000	39.000	32.000	39.000
Wilcoxon W	82.000	94.000	87.000	94.000
Z	-1.470	-.490	-1.061	-.490
Asymp. Sig. (2-tailed)	.142	.624	.288	.624

Table 9: Mann-Whitney U Test between the unaffected CST FA of patients and bilateral mean CST FA of controls.

	TMeanC FA	MeanC FA	TMaxC FA	MaxC FA
Mann-Whitney U	4.000	25.000	9.000	25.000
Wilcoxon W	59.000	80.000	64.000	80.000
Z	-3.348	-1.633	-2.939	-1.633
Asymp. Sig. (2-tailed)	.001	.102	.003	.102

Table 10: Mann-Whitney U Test between affected side CST FA / unaffected side CST FA of patients and left CST FA value/right CST FA value in controls.

Correlation among the affected CST FA values and the clinical-neurophysiological scores

A correlation statistical analysis was performed among the FA values calculated on the TMeanCs, MeanCs, TMaxCs and MaxCs of patients' affected CST, and the clinical and neurophysiological score.

For each clinical and neurophysiological scores, 3 values were considered:

1. **Baseline** (T0), corresponding to the value recorded prior to treatment;
2. **Delta**, corresponding to the absolute change in scores after treatment (T1 minus T0);
3. **Ratio**, corresponding to the ratio of the difference between the score recorded in T1 minus that recorded at T0 one, and the sum of the score recorded at T1 and T0; simplifying, ratio will correspond to (T1 value - T0 value / T1 value + T0 value). This value will provide a measure of relative change, taking into account baseline status.

That means that, for example, we considered 3 values for the ARAT assessment:

- ARAT T0, corresponding to the "starting point" value recorded at T0:
- ARAT delta, corresponding to the "absolute" variation between the T1 and T0 assessments;
- ARAT ratio, corresponding to the rate of variation between T1 and T0.

Each of these values were compared with the FA value calculated on the TMeanC, MeanC, TMaxC and MaxC of the patients' affected CST. Moreover, each all the clinical and neurophysiological data were also correlate with the following FA values

ratio (unaffected CST - affected CST)/(unaffected CST + affected CST), as seen in a previous paper (15).

This ratio (from now on named FAratio) was executed for the FA values calculated on all the 4 types of connectivity maps we considered, the unthresholded maximum ones, the thresholded maximum ones, the unthresholded mean ones and the thresholded mean ones, It gave rise to 4 values, named FAratio TMeanC, FAratio MeanC, FA ratio TMaxC and FA ratio MaxC.

The aim of calculating the ratios is to normalize the raw FA value of the affected FA with the controlateral one.

During the correlation analysis between JTT and FA values, patient 6 was excluded because of the fact that he could not perform anything when he was assessed during the basal evaluation.

During the correlation analysis between Aslope and FA values, patient 3, 6 and 10 were excluded because of the fact that no MEP could be recorded in the basal and in the follow-up evaluation.

A synopsis of this analysis is showed in table 11.

The following statistically significant correlations were observed:

- ARAT delta with MeanC, TMaxC and MaxC;
- ARAT ratio with TMeanC, MeanC, TMaxC, MaxC and FAratioTMaxC;
- GRIP T0 with FAratioMeanC and FAratioMaxC;
- Aslope delta with FAratioTMeanC, FAratioMeanC and FAratioMaxC.
- MAXdelta and MAXratio with FAratioMeanC and FAratioMaxC

Their plots are shown in the figures 13 – 29.

		ARATT0	ARATdelta	ARATratio	HPTT0	HPTdelta	HPTratio	JTTT0	JTTdelta	JTTratio	GRIPT0	GRIPdelta	GRIPratio	AslopeT0	Aslopedelta	Asloperatio	MAXT0	MAXdelta	MAXratio
TMeanC	Correlation Coefficient	.371	-.505	-.661(*)	-.261	.091	.042	.300	-.600	-.600	-.406	.079	.042	-.143	-.643	-.357	-.423	-.092	-.092
	Sig. (2-tailed)	.291	.137	.038	.467	.803	.907	.433	.088	.088	.244	.829	.907	.760	.119	.432	.223	.800	.800
	N	10	10	10	10	10	10	9	9	9	10	10	10	7	7	7	10	10	10
MeanC	Correlation Coefficient	.292	-.705(*)	-.758(*)	-.382	-.115	.042	.450	-.333	-.367	-.455	-.018	-.030	-.464	-.536	-.179	-.399	-.129	-.129
	Sig. (2-tailed)	.413	.023	.011	.276	.751	.907	.224	.381	.332	.187	.960	.934	.294	.215	.702	.254	.723	.723
	N	10	10	10	10	10	10	9	9	9	10	10	10	7	7	7	10	10	10
TMaxC	Correlation Coefficient	.340	-.669(*)	-.733(*)	-.358	.079	.091	.350	-.433	-.467	-.382	.079	.042	-.393	-.607	-.321	-.423	-.104	-.104
	Sig. (2-tailed)	.336	.035	.016	.310	.829	.803	.356	.244	.205	.276	.829	.907	.383	.148	.482	.223	.774	.774
	N	10	10	10	10	10	10	9	9	9	10	10	10	7	7	7	10	10	10
MaxC	Correlation Coefficient	.292	-.705(*)	-.758(*)	-.382	-.115	.042	.450	-.333	-.367	-.455	-.018	-.030	-.464	-.536	-.179	-.399	-.129	-.129
	Sig. (2-tailed)	.413	.023	.011	.276	.751	.907	.224	.381	.332	.187	.960	.934	.294	.215	.702	.254	.723	.723
	N	10	10	10	10	10	10	9	9	9	10	10	10	7	7	7	10	10	10
FAratioTMeanC	Correlation Coefficient	-.316	.371	.539	.224	-.176	-.079	-.183	.617	.633	.394	-.176	-.127	-.071	.786(*)	.571	.301	.264	.264
	Sig. (2-tailed)	.374	.291	.108	.533	.627	.829	.637	.077	.067	.260	.627	.726	.879	.036	.180	.399	.461	.461
	N	10	10	10	10	10	10	9	9	9	10	10	10	7	7	7	10	10	10
FAratioMeanC	Correlation Coefficient	.243	.359	.115	.588	.115	-.358	-.550	.433	.467	.758(*)	-.055	-.091	.036	.821(*)	.679	.153	.742(*)	.742(*)
	Sig. (2-tailed)	.498	.309	.751	.074	.751	.310	.125	.244	.205	.011	.881	.803	.939	.023	.094	.672	.014	.014
	N	10	10	10	10	10	10	9	9	9	10	10	10	7	7	7	10	10	10
FAratioTMaxC	Correlation Coefficient	-.498	.474	.636(*)	.042	-.406	-.018	-.183	.583	.583	.152	-.188	-.152	.321	.429	.143	.460	-.166	-.166
	Sig. (2-tailed)	.143	.166	.048	.907	.244	.960	.637	.099	.099	.676	.603	.676	.482	.337	.760	.181	.647	.647
	N	10	10	10	10	10	10	9	9	9	10	10	10	7	7	7	10	10	10
FAratioMaxC	Correlation Coefficient	.243	.359	.115	.588	.115	-.358	-.550	.433	.467	.758(*)	-.055	-.091	.036	.821(*)	.679	.153	.742(*)	.742(*)
	Sig. (2-tailed)	.498	.309	.751	.074	.751	.310	.125	.244	.205	.011	.881	.803	.939	.023	.094	.672	.014	.014
	N	10	10	10	10	10	10	9	9	9	10	10	10	7	7	7	10	10	10

Table 11. Blue: correlation is significant at the 0.05 level (2-tailed). Pink: correlation is significant at the 0.1 level (2-tailed).

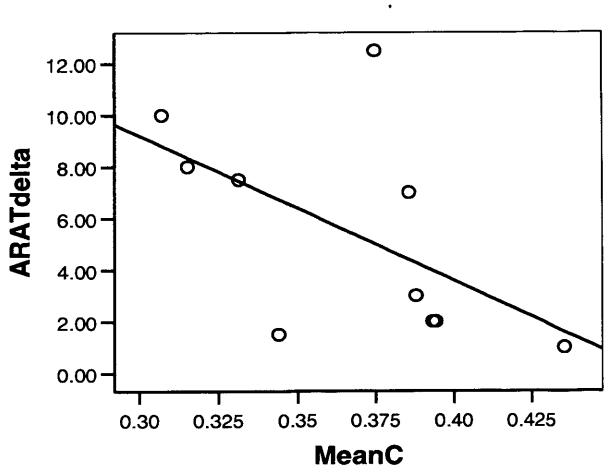

Figure 13: Plot of ARAT delta versus FA values calculated on the unthresholded mean connectivity maps in the in the whole group of patients.

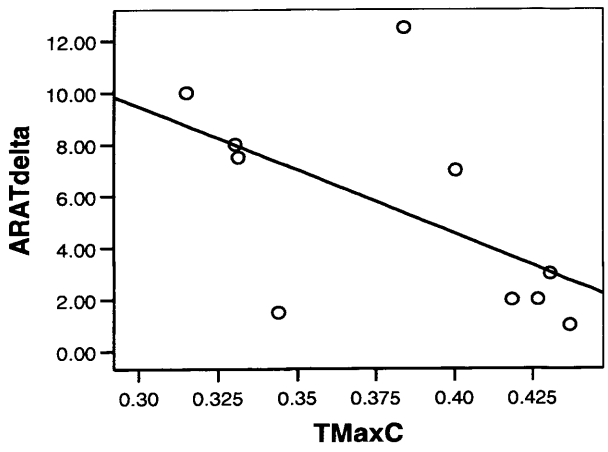

Figure 14: Plot of ARAT delta versus FA values calculated on the thresholded maximum connectivity maps in the in the whole group of patients.

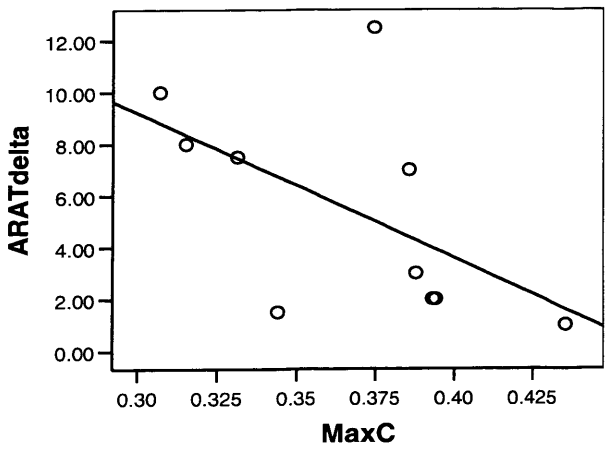

Figure 15: Plot of ARAT delta versus FA values calculated on the unthresholded maximum connectivity maps in the in the whole group of patients.

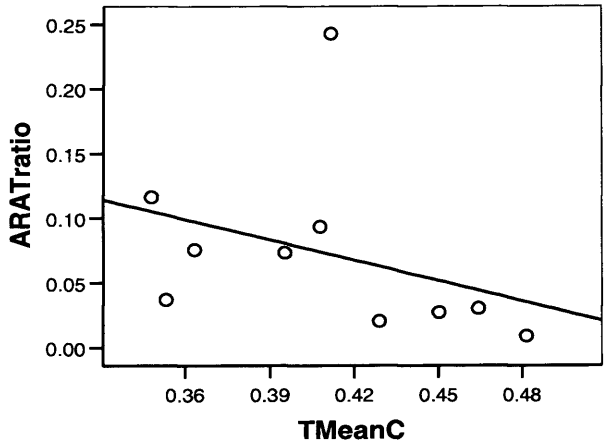

Figure 16: Plot of ARAT ratio versus FA values calculated on the thresholded mean connectivity maps in the in the whole group of patients.

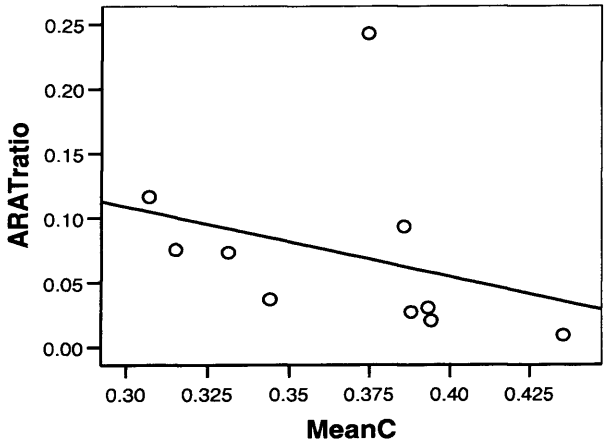

Figure 17: Plot of ARAT ratio versus FA values calculated on the unthresholded mean connectivity maps in the in the whole group of patients.

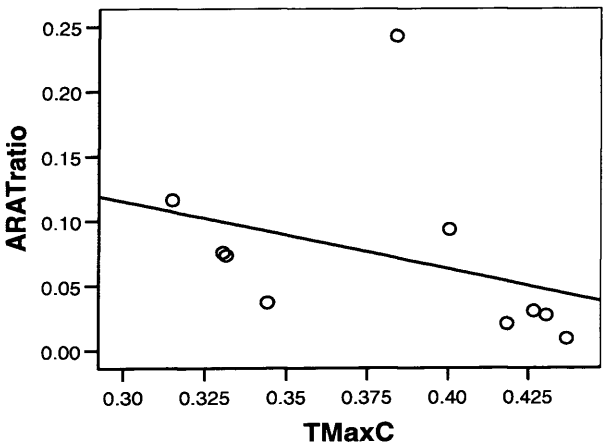

Figure 18: Plot of ARAT ratio versus FA values calculated on the thresholded maximum connectivity maps in the in the whole group of patients.

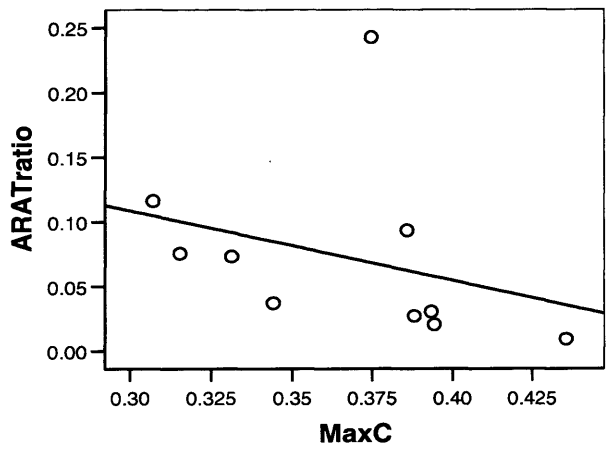

Figure 19: Plot of ARAT ratio versus FA values calculated on the unthresholded maximum connectivity maps in the in the whole group of patients.

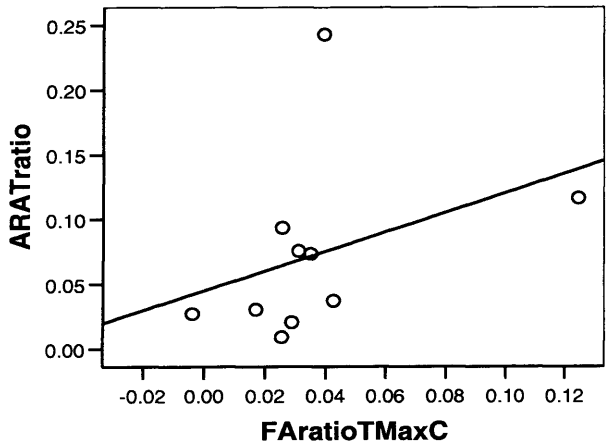

Figure 20: Plot of ARAT ratio versus FAratioTMaxC

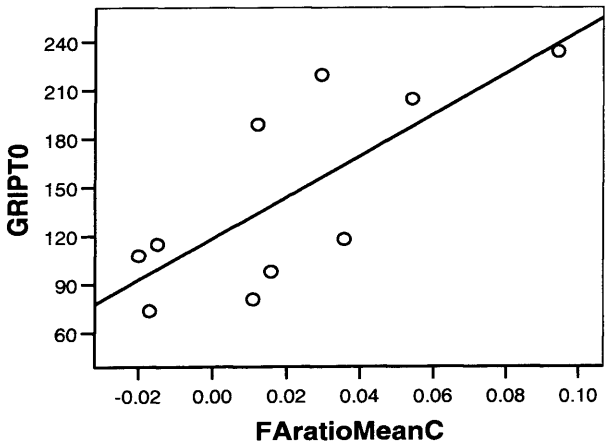

Figure 21: Plot of GRIP T0 versus FAratioMeanC in the in the whole group of patients.

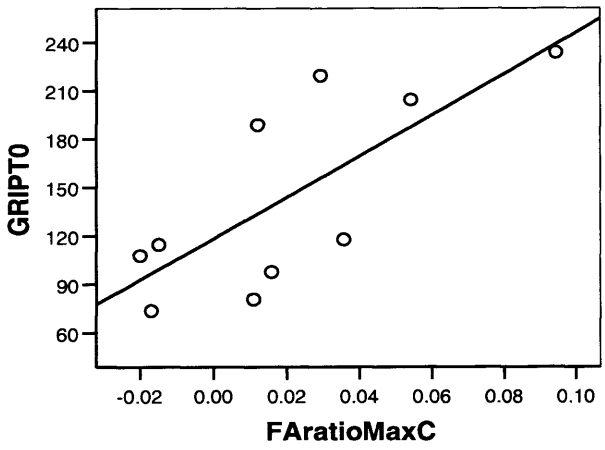

Figure 22: Plot of GRIP T0 versus FAratioTMaxC in the in the whole group of patients.

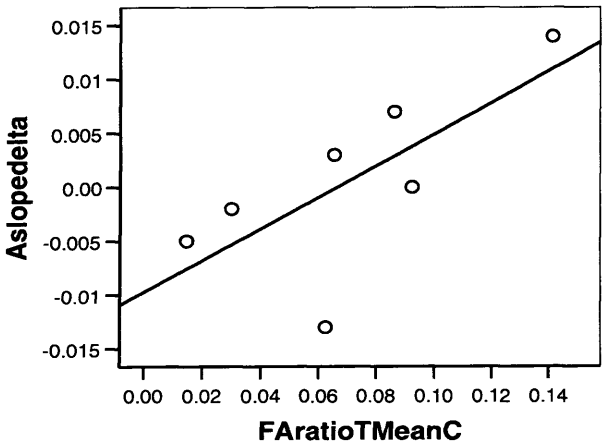

Figure 23: Plot of Aslope delta versus FAratioTMeanC in the in the whole group of patients.

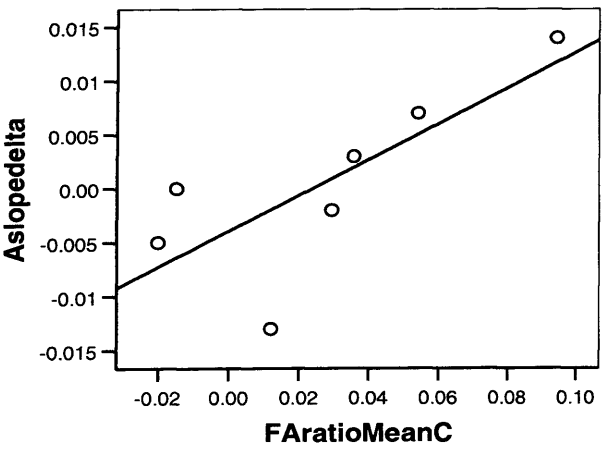

Figure 24: Plot of Aslope delta versus FAratio MeanC in the in the whole group of patients.

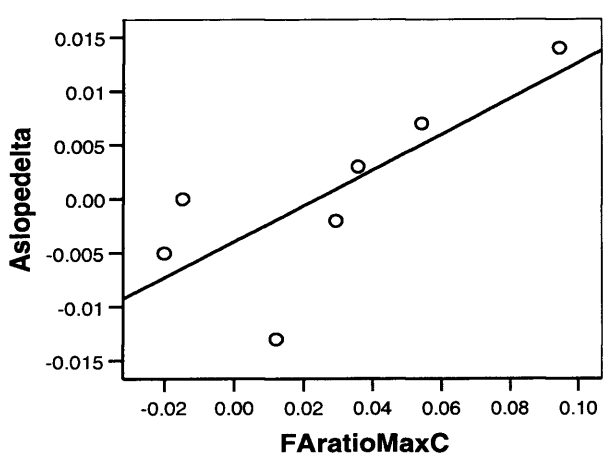

Figure 25: Plot of Aslope delta versus FAratio MaxC in the in the whole group of patients.

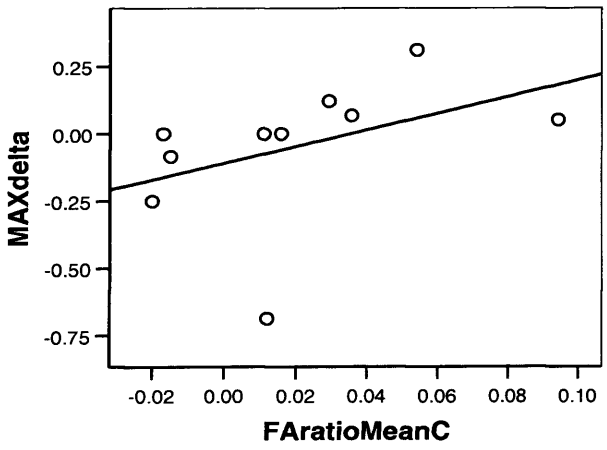

Figure 26: Plot of MAXdelta versus FAratio MeanC in the in the whole group of patients.

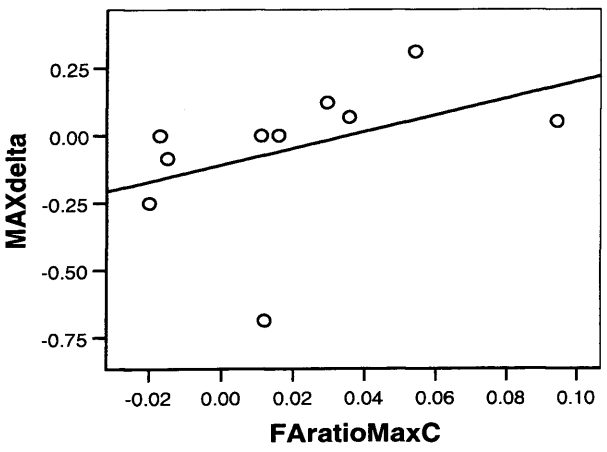

Figure 27: Plot of MAXdelta versus FAratio MaxC in the in the whole group of patients.

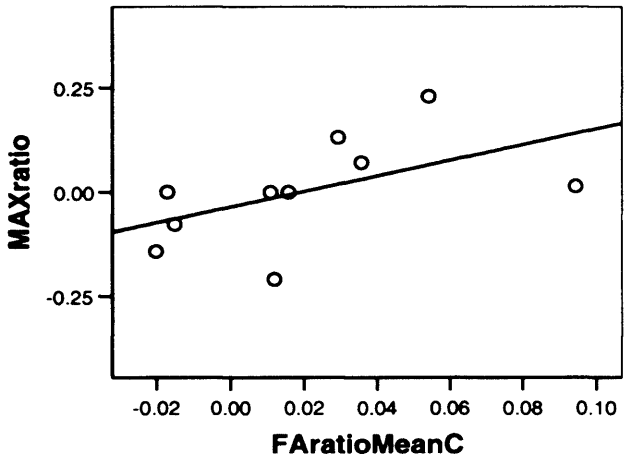

Figure 28: Plot of MAXratio versus FAratioMeanC in the in the whole group of patients.

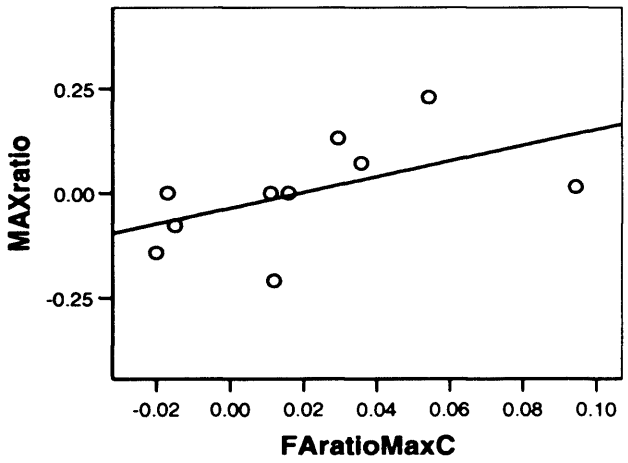

Figure 29: Plot of MAXratio versus FAratioMaxC in the in the whole group of patients.

Discussion

To our knowledge, our study is the first which investigated and highlighted the existence of a correlation between the values of FA calculated on the whole telencephalic portion of the CST, and clinical and neurophysiological outcomes assessed before and after a rehabilitative treatment in chronic stroke patients.

Our study confirms the findings of numerous papers about the reliability of FA as a measure for assessing the integrity of CST in patient previously affected from a stroke (61).

However, we decided to consider the value of FA within the whole CST telencephalic portion, since it probably allows a better and more global assessment of CST integrity.

Indeed, according to the results of our statistical analysis, FA computed on CST probabilistic tractography was able to distinguish between the affected and unaffected CSTs of patients calculated on TMeanCs (see table 6). It was able as well to distinguish between the affected CST of patients and the bilateral mean CST FA of controls through the values calculated on TMeanCs and TMaxCs, but not on those calculated on MeanCs and MaxCs (see table 8).

We got the same result when we tried to differentiate patients and controls not through the FA raw values, but through the ratios of affected/unaffected patients' CST FA values and left/right controls' CST FA: TMeanCs and TMaxCs FA values were statistically different between the two groups, but MeanCs and MaxCs FA values were not (see table 10). We thought it was reasonable to compare affected/unaffected

patients' CSTs with left/right controls' CSTs because no statistical difference in FA values could be spotted between the left and right side of controls (see table 7).

Conversely, the statistical analysis among all the FA values of all the unaffected CSTs (in patients and controls group) revealed no significant difference for all the connectivity maps (see table 9).

In the light of what we said above, we can state that, in our patients and controls, the FA values of the CST whole telencephalic portion with the best sensibility/specificity ratio are the ones calculated on the thresholded mean and maximum connectivity maps. Probably the FA values calculated on the thresholded mean connectivity maps are slightly superior to those calculated on the thresholded maximum connectivity maps (see Table6). On the other hand, FA values calculated on the unthresholded maps did not show the same reliability.

According to what we have just stated, for the purpose of the next part of the discussion we shall consider mainly the FA values derived from the thresholded connectivity maps, that are displayed in table 11 in the rows for TmeanC, TMaxC, FAratioTMeanC and FAratioTMaxC.

Since it appears that, according to the others' previous findings (62, 63), FA is a continuous variable able to detect, through its decrease, the damage of the CST, it seems also reasonable to suppose that a correlation between the decrease of FA (assessed through probabilistic tractography) and the other clinical and neurophysiological consequences of a CST disruption might exist.

Moreover, the degree of CST disruption might also predict the eventually gained motor recovery after the two weeks of intensive upper limb rehabilitative treatment, as already observed in 2007 (15).

The results of our pilot study were slightly different from our a priori hypothesis. FAratio meanC and FAratio MaxC showed a very good linear correlation with the degree of strength exerted by the patients through the manipulandum at T0 (see figure 21 and 22), with a p value < 0.05. It sounds reasonable that, before starting the rehabilitative treatment, the integrity of the CST crossed fibres, which are crucial for the motility of the most distal part of the limbs, correlates very well with the strength exerted by the patients through the manipulandum.

At first sight, you can suppose you will see a similar correlation in the degree of recovery gained by the patient after the rehabilitation: the more is the integrity of his CST, the better he will perform after the treatment.

Surprisingly, apart from Aslope delta, among all the delta and ratio parameters (the ones that reveals the "absolute" and the "relative" value of recovery degree achieved by the patient) which reached a statistically significant correlation with the thresholded FA values, only ARATratio showed a positive linear correlation toward FAratioTMaxC: its correlation with TMeanC and TMaxC was negative. In the same manner, ARATdelta showed a negative correlation with TMaxC. Actually, we have to say that we are quite sure that, generally speaking, a decrease in the FA value indicates a degeneration of the CST, but we are just starting to use this protocol, and more experience is needed for a real understanding of what it means to measure FA in

different ways. Anyway, we tried to formulate an explanation for this negative correlation.

It is possible that the patients who benefited most from the rehabilitation are those with a "medium" disruption of the CST. This is because patients with a very important stroke, which destroyed almost completely their CST, no matter how much they will struggle, their recovery will be very poor.

Similarly, patients with a very mild stroke, with a minimum CST disruption, will not improve very much in the assessment scores, simply because they have a minor margin of recovery. So we can hypothesize that patients with a clinically important motor impairment, but still possessing a relatively good CST integrity, will improve during the rehabilitative treatment more than the others.

The use of a quadratic correlation, instead of a linear one, displays better this concept (see figure 30): the correlation appears U-shaped, and shows better our idea. It is easy to agree that a larger number of patients is needed for confirming our hypothesis because at the moment, with a so small sample, a couple of new patients could alter the aspect of that correlation. However, we think that this supposition has a good logical basis.

Some biases are probably present in our study.

A possible one is the selection of the patient. They were homogeneous neither for age (range 40 - 77 years) nor for the time between the acute phase of the stroke and the start of assessment and rehabilitation (range 13 - 288 months).

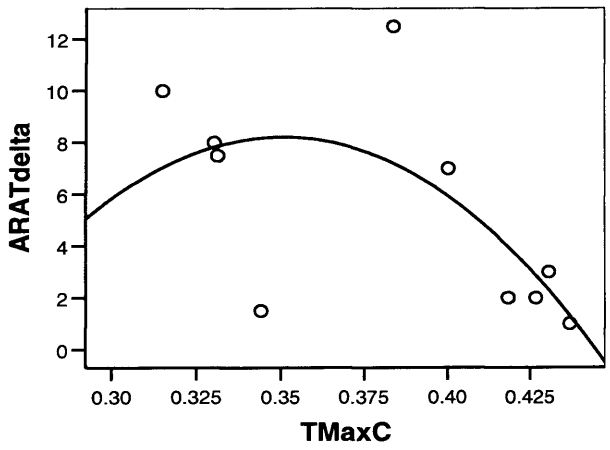

A

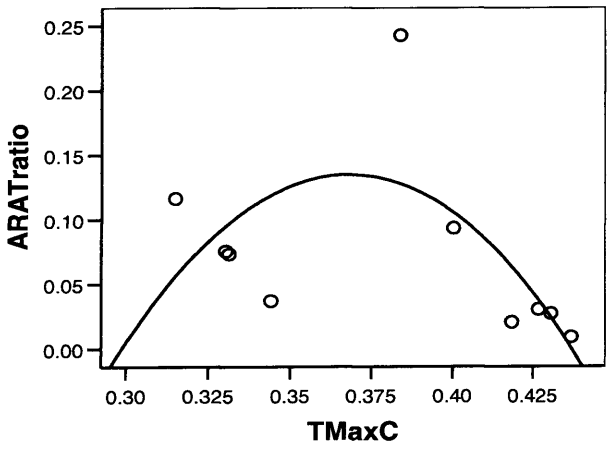

C

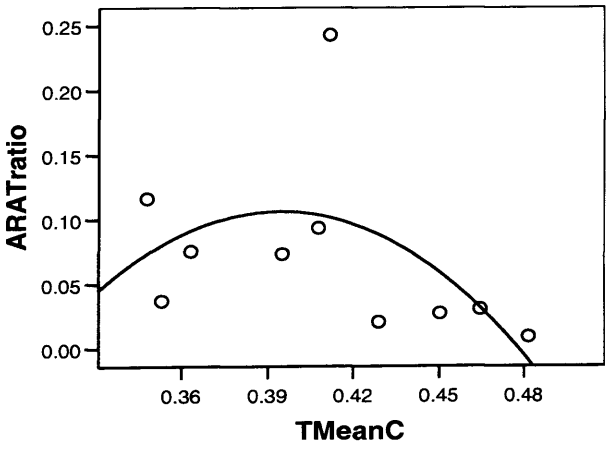

D

Figure 30: Quadratic correlation of ARAT delta versus TMaxC (A), and ARAT ratio versus TMaxC (B),and TMeanC (D).

Time after the acute phase has probably played an important part; recently, some authors published a study which related CST excitability measures with clinical function in a group of 10 patients: CST integrity correlated well with hand function in the 3 months following the stroke, but not in the following period (65). Globally, for most of the patients, we cannot deny that the treatment was of benefit in the patients group (e.g. in the ARAT test the mean improvement between T0 and T1 was about 10% for the whole group). However, the tests chosen as "markers" for an eventual improvement after the rehabilitation would have been verisimilarly more sensible with less chronic patients.

It is also fair to hypothesize that younger brains can perform a better recovery after an insult; from a logical point of view you can guess that between two patients, with a similar extension and localization of the stroke, with a similar CST disruption assessed by probabilistic tractography FA values, with similar scores achieved in all the tests at T0, the younger one will recover better than the older one.

For this reason, a larger number of patients could allow us to stratify the patients according to their age while performing the statistical evaluation. Moreover, concomitant disorders or treatments, especially in the most elderly, could have influenced the degree of recovery after the intensive upper limbs rehabilitation (66).

The brain can try to amend a damage following a stroke in several ways: remodelling of the motor pathway from the unaffected motor cortex to the affected hand, with peri-lesional reorganization, thanks to the recovery of a damaged lateral CST, or with the contribution of the secondary motor area (64). All these different mechanisms probably act in a parallel than in a serial way. It means that each of them make the scene

probably contemporarily, even if with different degrees, and not one consecutively to the other one. Different rehabilitative treatment could tend to enhance one mechanism rather than another one, rendering less crucial the CST integrity or, anyway, leading the brain to a certain kind of recovery for whom, maybe, a certain degree of CST disruption could be uninfluential, or even favourable.

Summarizing, the following main points of the study should be modified:

- The recruitment of the patients should be extended also to those who suffered from stroke in the last 6-12 months;
- A larger number of cases should be recruited would allow to better characterize different clusters (e.g. age, sex, concomitant disorders, etiopathology of the stroke etc.) inside the same group of patients;
- Different rehabilitative strategies should be set, in order to detect different indications for different kind of patients.

These amended criteria will presumably render this study more able to investigate the underlying mechanisms of after stroke recovery through all the potentialities of probabilistic tractography.

It is worth highlighting one last point: the protocol used during this study for the execution of probabilistic tractography was aimed to render automated all the steps regarding the realizations of the ROIs. We sought to perform all our measurements in an automated way unbiased by manual ROIs drawing in order to achieve a high degree of reliability and reproducibility. Indeed, the motor cortex ROIs were extracted through Freesurfer, whilst the ones for the cerebral peduncle were drawn manually in a standardised space, and "transferred" to the subject's specific native space thanks

to SPM5. In our opinion, this approach is crucial in avoiding most of the operator-dependent biases during the determination of the ROIs.

Reference List

(1) *Dobkin BH. Clinical practice. Rehabilitation after stroke. N Engl J Med 2005 Apr 21;352:1677-1684.*

(2) *Helgason CM, Wolf PA. American Heart Association Prevention Conference IV: prevention and rehabilitation of stroke: executive summary. Circulation 1997 Jul 15;96:701-707.*

(3) *Sacco RL. Newer risk factors for stroke. Neurology 2001;57:S31-S34.*

(4) *Jorgensen HS, Nakayama H, Raaschou HO, Olsen TS. Intracerebral hemorrhage versus infarction: stroke severity, risk factors, and prognosis. Ann Neurol 1995 Jul;38:45-50.*

(5) *Murray CJ, Lopez AD. Global mortality, disability, and the contribution of risk factors: Global Burden of Disease Study. Lancet 1997 May 17;349:1436-1442.*

(6) *Lopez AD, Mathers CD, Ezzati M, Jamison DT, Murray CJ. Global and regional burden of disease and risk factors, 2001: systematic analysis of population health data. Lancet 2006 May 27;367:1747-1757.*

(7) *Organised inpatient (stroke unit) care for stroke. Stroke Unit Trialists' Collaboration. Cochrane Database Syst Rev 2000;CD000197.*

(8) *Ward NS, Frackowiak RS. The functional anatomy of cerebral reorganisation after focal brain injury. J Physiol Paris 2006 Jun;99:425-436.*

(9) *Muller K, Kass-Iliyya F, Reitz M. Ontogeny of ipsilateral corticospinal projections: a developmental study with transcranial magnetic stimulation. Ann Neurol 1997 Nov;42:705-711.*

(10) *Ago T, Kitazono T, Ooboshi H, et al. Deterioration of pre-existing hemiparesis brought about by subsequent ipsilateral lacunar infarction. J Neurol Neurosurg Psychiatry 2003 Aug;74:1152-1153.*

(11) *Fujii Y, Nakada T. Cortical reorganization in patients with subcortical hemiparesis: neural mechanisms of functional recovery and prognostic implication. J Neurosurg 2003 Jan;98:64-73.*

(12) *Ward NS, Brown MM, Thompson AJ, Frackowiak RS. Neural correlates of motor recovery after stroke: a longitudinal fMRI study. Brain 2003 Nov;126:2476-2496.*

(13) *Rossini PM, Altamura C, Ferreri F, et al. Neuroimaging experimental studies on brain plasticity in recovery from stroke. Eura Medicophys 2007 Jun;43:241-254.*

(14) *Ward NS, Newton JM, Swayne OB, et al. Motor system activation after subcortical stroke depends on corticospinal system integrity. Brain 2006 Mar;129:809-819.*

(15) *Stinear CM, Barber PA, Smale PR, Coxon JP, Fleming MK, Byblow WD. Functional potential in chronic stroke patients depends on corticospinal tract integrity. Brain 2007 Jan;130:170-180.*

(16) *Einstein A. Investigations on the theory of the Brownian movement. In: Dutton, ed. New York: 1926.*

(17) *Neil JJ. Diffusion imaging concepts for clinicians. J Magn Reson Imaging 2008 Jan;27:1-7.*

(18) *Le BD. Looking into the functional architecture of the brain with diffusion MRI. Nat Rev Neurosci 2003 Jun;4:469-480.*

(19) *Hagmann P, Jonasson L, Maeder P, Thiran JP, Wedeen VJ, Meuli R. Understanding diffusion MR imaging techniques: from scalar diffusion-weighted imaging to diffusion tensor imaging and beyond. Radiographics 2006 Oct;26 Suppl 1:S205-S223.*

(20) *Tuch DS, Reese TG, Wiegell MR, Makris N, Belliveau JW, Wedeen VJ. High angular resolution diffusion imaging reveals intravoxel white matter fiber heterogeneity. Magn Reson Med 2002 Oct;48:577-582.*

(21) *Johansen-Berg H, Behrens TE. Just pretty pictures? What diffusion tractography can add in clinical neuroscience. Curr Opin Neurol 2006 Aug;19:379-385.*

(22) *Ramu J, Herrera J, Grill R, Bockhorst T, Narayana P. Brain fiber tract plasticity in experimental spinal cord injury: diffusion tensor imaging. Exp Neurol 2008 Jul;212:100-107.*

(23) *Vargas MI, Delavelle J, Jlassi H, et al. Clinical applications of diffusion tensor tractography of the spinal cord. Neuroradiology 2008 Jan;50:25-29.*

(24) *Aoki S, Iwata NK, Masutani Y, et al. Quantitative evaluation of the pyramidal tract segmented by diffusion tensor tractography: feasibility study in patients with amyotrophic lateral sclerosis. Radiat Med 2005 May;23:195-199.*

(25) *Bozzali M, Cherubini A. Diffusion tensor MRI to investigate dementias: a brief review. Magn Reson Imaging 2007 Jul;25:969-977.*

(26) *Matsuo K, Mizuno T, Yamada K, et al. Cerebral white matter damage in frontotemporal dementia assessed by diffusion tensor tractography. Neuroradiology 2008 Jul;50:605-611.*

(27) *Nestor PG, Kubicki M, Niznikiewicz M, Gurrera RJ, McCarley RW, Shenton ME. Neuropsychological disturbance in schizophrenia: a diffusion tensor imaging study. Neuropsychology 2008 Mar;22:246-254.*

(28) *Ludeman NA, Berman JI, Wu YW, et al. Diffusion tensor imaging of the pyramidal tracts in infants with motor dysfunction. Neurology 2008 Apr 30.*

(29) *Ahn YH, Ahn SH, Kim H, Hong JH, Jang SH. Can stroke patients walk after complete lateral corticospinal tract injury of the affected hemisphere? Neuroreport 2006 Jul 17;17:987-990.*

(30) *Jang SH, You SH, Kwon YH, Hallett M, Lee MY, Ahn SH. Cortical reorganization associated lower extremity motor recovery as evidenced by functional MRI and diffusion tensor tractography in a stroke patient. Restor Neurol Neurosci 2005;23:325-329.*

(31) *Jang SH, Kim SH, Cho SH, Choi BY, Cho YW. Demonstration of motor recovery process in a patient with intracerebral hemorrhage. NeuroRehabilitation 2007;22:141-145.*

(32) *Lai C, Zhang SZ, Liu HM, et al. White matter tractography by diffusion tensor imaging plays an important role in prognosis estimation of acute lacunar infarctions. Br J Radiol 2007 Oct;80:782-789.*

(33) *Parmar H, Golay X, Lee KE, Hui F, Sitoh YY. Early experiences with diffusion tensor imaging and magnetic resonance tractography in stroke patients. Singapore Med J 2006 Mar;47:198-203.*

(34) *Rovaris M, Filippi M. Diffusion tensor MRI in multiple sclerosis. J Neuroimaging 2007 Apr;17 Suppl 1:27S-30S.*

(35) *Lo CY, Chao YP, Chou KH, Guo WY, Su JL, Lin CP. DTI-based virtual reality system for neurosurgery. Conf Proc IEEE Eng Med Biol Soc 2007;2007:1326-1329.*

(36) *Romano A, Ferrante M, Cipriani V, et al. Role of magnetic resonance tractography in the preoperative planning and intraoperative assessment of patients with intra-axial brain tumours. Radiol Med (Torino) 2007 Sep;112:906-920.*

(37) *Wei CW, Guo G, Mikulis DJ. Tumor effects on cerebral white matter as characterized by diffusion tensor tractography. Can J Neurol Sci 2007 Feb;34:62-68.*

(38) *Beaulieu C. The basis of anisotropic water diffusion in the nervous system - a technical review. NMR Biomed 2002 Nov;15:435-455.*

(39) *Lazar M, Alexander AL. An error analysis of white matter tractography methods: synthetic diffusion tensor field simulations. Neuroimage 2003 Oct;20:1140-1153.*

(40) *Reese TG, Heid O, Weisskoff RM, Wedeen VJ. Reduction of eddy-current-induced distortion in diffusion MRI using a twice-refocused spin echo. Magn Reson Med 2003 Jan;49:177-182.*

(41) *Wheeler-Kingshott CA, Hickman SJ, Parker GJ, et al. Investigating cervical spinal cord structure using axial diffusion tensor imaging. Neuroimage 2002 May;16:93-102.*

(42) *Jansons KM, Alexander DC. Persistent Angular Structure: new insights from diffusion MRI data. Dummy version. Inf Process Med Imaging 2003 Jul;18:672-683.*

(43) *Basser PJ, Mattiello J, LeBihan D. Estimation of the effective self-diffusion tensor from the NMR spin echo. J Magn Reson B 1994 Mar;103:247-254.*

(44) *Deichmann R, Schwarzbauer C, Turner R. Optimisation of the 3D MDEFT sequence for anatomical brain imaging: technical implications at 1.5 and 3 T. Neuroimage 2004 Feb;21:757-767.*

(45) *Desikan RS, Segonne F, Fischl B, et al. An automated labeling system for subdividing the human cerebral cortex on MRI scans into gyral based regions of interest. Neuroimage 2006 Jul 1;31:968-980.*

(46) *Behrens TE, Johansen-Berg H, Woolrich MW, et al. Non-invasive mapping of connections between human thalamus and cortex using diffusion imaging. Nat Neurosci 2003 Jul;6:750-757.*

(47) *Ashburner J, Friston KJ. Unified segmentation. Neuroimage 2005 Jul 1;26:839-851.*

(48) *Parker GJ, Alexander DC. Probabilistic anatomical connectivity derived from the microscopic persistent angular structure of cerebral tissue. Philos Trans R Soc Lond B Biol Sci 2005 May 29;360:893-902.*

(49) *Parker GJ, Alexander DC. Probabilistic Monte Carlo based mapping of cerebral connections utilising whole-brain crossing fibre information. Inf Process Med Imaging 2003 Jul;18:684-695.*

(50) *Cook PA, Zhang H, Avants BB, et al. An automated approach to connectivity-based partitioning of brain structures. Med Image Comput Comput Assist Interv Int Conf Med Image Comput Comput Assist Interv 2005;8:164-171.*

(51) *Alexander DC, Barker GJ, Arridge SR. Detection and modeling of non-Gaussian apparent diffusion coefficient profiles in human brain data. Magn Reson Med 2002 Aug;48:331-340.*

(52) *Tuch DS, Wedeen VJ, Dale AM, George JS, Belliveau JW. Conductivity tensor mapping of the human brain using diffusion tensor MRI. Proc Natl Acad Sci U S A 2001 Sep 25;98:11697-11701.*

(53) *Cook PA, Alexander DC, Parker GJM. Modelling noise-induced fibre-orientation error in diffusion-tensor MRI. IEEE International Symposium on Biomedical Imaging 2004:332-335.*

(54) *Pierpaoli C, Basser PJ. Toward a quantitative assessment of diffusion anisotropy. Magn Reson Med 1996 Dec;36:893-906.*

(55) *Pierpaoli C, Jezzard P, Basser PJ, Barnett A, Di CG. Diffusion tensor MR imaging of the human brain. Radiology 1996 Dec;201:637-648.*

(56) *Noskin O, Krakauer JW, Lazar RM, et al. Ipsilateral motor dysfunction from unilateral stroke: implications for the functional neuroanatomy of hemiparesis. J Neurol Neurosurg Psychiatry 2008 Apr;79:401-406.*

(57) *Lyle RC. A performance test for assessment of upper limb function in physical rehabilitation treatment and research. Int J Rehabil Res 1981;4:483-492.*

(58) *Yozbatiran N, Der-Yeghiaian L, Cramer SC. A standardized approach to performing the action research arm test. Neurorehabil Neural Repair 2008 Jan;22:78-90.*

(59) *Hummel F, Celnik P, Giraux P, et al. Effects of non-invasive cortical stimulation on skilled motor function in chronic stroke. Brain 2005 Mar;128:490-499.*

(60) *Stern EB. Stability of the Jebsen-Taylor Hand Function Test across three test sessions. Am J Occup Ther 1992 Jul;46:647-649.*

(61) *Ciccarelli O, Catani M, Johansen-Berg H, Clark C, Thompson A. Diffusion-based tractography in neurological disorders: concepts, applications, and future developments. Lancet Neurol 2008 Aug;7:715-727.*

(62) *Newton JM, Ward NS, Parker GJ, et al. Non-invasive mapping of corticofugal fibres from multiple motor areas--relevance to stroke recovery. Brain 2006 Jul;129:1844-1858.*

(63) *Jang SH, Bai D, Son SM, et al. Motor outcome prediction using diffusion tensor tractography in pontine infarct. Ann Neurol 2008 Jul 25.*

(64) *Jang SH. A review of motor recovery mechanisms in patients with stroke. NeuroRehabilitation 2007;22:253-259.*

(65) *Swayne OB, Rothwell JC, Ward NS, Greenwood RJ. Stages of motor output reorganization after hemispheric stroke suggested by longitudinal studies of cortical physiology. Cereb Cortex 2008 Aug;18:1909-1922.*

(66) *Cramer SC. Repairing the human brain after stroke. II. Restorative therapies. Ann Neurol 2008 May;63:549-560.*